Supporting Information

Solid-Phase Synthesis of Titanium-Oxo Clusters and Their Unprecedented Catalytic Performance in Oxidative Desulfurization of Fuel Oil

Xinchun Liu,[a] Yanpeng Yuan,[a] Jiawei Fu,[a] Yuqing Kong,[a] Yinyong Sun,*[a] Xiaolin Li,*[b] and Nan Qu[c]

[a] MIIT Key Laboratory of Critical Materials Technology for New Energy Conversion and Storage, School of Chemistry and Chemical Engineering, Harbin Institute of Technology, Harbin 150001, China

[b] Institute of Intelligent Manufacturing Technology, Shenzhen Polytechnic, Shenzhen 518055, China

[c] School of Materials Science and Engineering, Harbin Institute of Technology, Harbin, 150001, China

* Corresponding author. E-mail: yysun@hit.edu.cn; lixiaolin0427@szpt.edu.cn

Table of Contents

1 Materials and Methods

1.1 Materials

Titanium ethoxide ($Ti(OEt)_4$), titanium isopropoxide ($Ti(O^iPr)_4$), 4-aminobenzoic acid (abz), 4-tert-butylbenzoic acid (tbbz)， biphenyl-4,4'-dicarboxylic acid (BPDC), $MnCl_2·4H_2O$, 1,4-benzenedicarboxylic acid (BDC), anhydrous ethanol, isopropanol, *n*-octane, benzothiophene (BT), dibenzothiophene (DBT), 4,6-dimethyldibenzothiophene (4,6-DMDBT), 5,5-dimethyl-1-pyrroline *N*-oxide (DMPO), tertiary butanol (TBA), *p*-benzoquinone (BQ), dimethyl sulfoxide (DMSO) were purchased from Beijing InnoChem Science & Technology Co., Ltd. Acetone was purchased from Adamas Biochemical Technology Co., Ltd. Hydrogen peroxide (H_2O_2, 30 wt%), was purchased from Aladdin Biochemical Technology Co., Ltd. All the chemicals and solvents were used as received without further purification.

1.2 Solid-phase synthesis of $Ti_6O_6(abz)_6(O^iPr)_6$

$Ti(O^iPr)_4$ (10 mmol, 3.0 mL) was taken by a pipette gun and immediately transferred into a 25 mL high-pressure autoclave (Anhui Kemi Machinery Technology Co., Ltd) at room temperature. Subsequently, abz (13.75 mmol, 1.886 g) was added and sealed. The autoclave was heated in an oven to 150 °C for 12 h. After cooling, the product obtained as bright yellow rod-like crystals $Ti_6O_6(abz)_6(O^iPr)_6$ [1] (named Ti_6abz_6) were washed fourth with 30 mL of isopropanol and dried at 60 °C for 12 h.

1.3 Solid-phase synthesis of $Ti_6O_6(4\text{-}tbbz)_6(O^iPr)_6$

Colorless rod-like crystals $Ti_6O_6(4\text{-}tbbz)_6(O^iPr)_6$[2] (named Ti_6tbbz_6) were synthesized by substituting abz with tbbz (15 mmol, 2.674 g) in the above synthetic procedure for Ti_6abz_6.

1.4 Solid-phase synthesis of $Ti_6O_6(4\text{-}tbbz)_{10}(O^iPr)_2$

Colorless needle-like crystals $Ti_6O_6(4\text{-}tbbz)_{10}(O^iPr)_2$[2] (named Ti_6tbbz_{10}) were synthesized by varying the dosage of $Ti(O^iPr)_4$ (3 mmol, 0.9 mL) and tbbz (24 mmol, 4.30 g) in the above synthetic procedure for Ti_6tbbz_6.

1.5 Solid-phase synthesis of $Ti_{29}KO_{39}(OEt)_{38}$

$Ti(OEt)_4$ (20 mmol, 4.2 mL) was taken by a pipette gun and immediately transferred into a 25 mL high-pressure autoclave at room temperature. Subsequently, BPDC (10 mmol, 2.422 g) was added and sealed. The autoclave was heated in an oven to 150 °C for 12 h. After cooling, the obtained product was washed with 30 mL of absolute ethanol (fourth), acetone (twice) and absolute ethanol (once) at room temperature, separately. Then, the obtained as colorless rhombic-like crystals $Ti_{29}KO_{39}(OEt)_{38}$ (named Ti_{29}) were dried at 60 °C for 12 h.

1.6 Preparation of MIL-125(Ti) with Ti_6abz_6

MIL-125(Ti) was synthesized using a modified method based on previous reports.[3] Ti_6abz_6 (0.167 mmol, 0.259 g) and BDC (6 mmol, 1 g) were added into a mixture solution containing 18 mL of DMF and 2 mL of methanol under vigorous agitation at room temperature. After stirring for 30 min, the mixture was transferred to a 50 mL Teflon-lined autoclave and placed in an oven at 150 °C for 24 h. After cooling, the obtained white solid was washed thoroughly with ethanol and then dried at 60 °C for 12 h.

1.7 Preparation of MUV-10(Ti, Mn) with Ti_6abz_6

MUV-10(Ti, Mn) was synthesized with Ti_6abz_6 according to the previously reported procedure.[4]

1.8 Physical and chemical characterization

Powder X-ray diffraction (XRD) patterns were recorded on a Bruker D8 advance diffractometer in Bragg-Brentano geometry equipped with a Ge-focusing primary monochromator (Cu-Kα radiation, $\lambda = 0.15406$ nm) at 40 kV and 40 mA with a scanning speed at 9° min^{-1} and a step size of 0.02°.

Scanning electron microscopy (SEM) images were obtained using a SUPRA 55 instrument with an acceleration voltage of 15 kV. SEM energy dispersive spectroscopy (EDS, Oxford Instrument) was used for composition analysis.

The diffuse ultraviolet-visible (UV-vis) spectra of all the samples were measured against

$BaSO_4$ in the region of 200-700 nm with a Hitachi UH4150 UV-VIS-NIR spectrophotometer.

Fourier transform infrared (FT-IR) spectra were collected in the range of 400-4000 cm^{-1} on the Thermo Fisher Scientific Nicolet iS20 spectrometer.

Raman spectra were acquired by a Horiba LabRAM HR Evolution Raman spectrometer using a 532 nm laser line.

The contact angle was measured using SL200B contact angle meter. The contact angle was measured by depositing water drops (4 μL / drop) at 3 different locations on each sample.

The N_2 adsorption-desorption isotherms were obtained at 77 K on a BSD-PS1 Static Volumetric Specific Surface and Aperture Analyzer. Before nitrogen adsorption, the samples were pretreated at 373K for 6 h under vacuum condition to remove the solvent molecules. The total surface area was calculated via the Brunauer-Emmett-Teller (BET) equation.

X-ray photoelectron spectrometer (XPS) was used to analyze chemical composition of all the samples on the Thermo Scientific K-Alpha spectrometer. The binding energy for Ti_{29} was based on the C 1s peak position at 284.8 eV. The binding energies of aromatic ring-rich Ti_6abz_6, Ti_6tbbz_6 and Ti_6tbbz_{10} were based on the C 1s peak position of 284.6 eV.

Thermogravimetric analysis (TGA) was performed on a HITACHI STA200 instrument under air conditions at a ramp rate of 10 °C/min.

The electron paramagnetic resonance (EPR) spectra were recorded on a Bruker A300 spectrometer at ambient temperature. The weight of all samples used to measure oxygen vacancies was 20 mg. The samples used to measure reactive oxygen species were prepared as follows. 10 mg of sample was dissolved in 2.5 mL of deionized water or anhydrous ethanol solution and mixed well by sonication, followed by the addition of 50 μL of H_2O_2 (30 wt.%) and 50 μL of 5,5'-dimethyl-1-pirroline-*N*-oxide (DMPO).

The inductively coupled plasma optical emission spectroscopy (ICP-OES) was conducted using an Avio 220 Max instrument.

Electrospray ionization mass spectrometry (ESI-MS) was carried out on an Agilent 6540

Q-TOF instrument. 20 mg of Ti_6tbbz_{10} was dissolved in 1 mL of dichloromethane and injected into ESI-MS port using positive-ion mode. Then 50 uL H_2O_2 was added to the above solution to test the intermediate catalysts.

Single-crystal diffraction data was collected on a Bruker D8 Venture diffractometer equipped with Mo-Kα X-ray source (λ = 0.71073 Å, monochromatic graphite) at room temperature. APEX2 program was used to record the number of data frames and the program SAINT routine in PEX2 was used for processing. Data were scaled and corrected for absorption effects using the multi-scan procedure as implemented in SADABS. The structure was solved by SHELXT-2018/2[5] and refined by full-matrix least-squares on F^2 using OLEX2[6] software package. All non-hydrogen atoms were refined by anisotropic displacement parameters. The coordinated ethoxide with huge thermal ellipsoid were refined by using EADP constraints to clear the warning of non-positive definite matrix. Hydrogen atoms were placed in geometrically suitable positions and refined riding with isotropic thermal parameter related to the equivalent isotropic thermal parameter of the parent atom. Crystallographic data of $Ti_{29}KO_{39}(OEt)_{38}$ (CCDC 2286846) had been deposited with the Cambridge Crystallographic Data Centre. Copy of data can be obtained free of charge on application to the CCDC, Cambridge, UK via https://www.ccdc.cam.ac.uk/structures/.

1.9 Catalytic tests

The oxidation of sulfocompound in model fuel was used as probe reaction to evaluate the catalytic performance of titanium-oxo clusters (TOCs). An amount of BT, DBT, or DMDBT dissolved in *n*-octane (1000 ppm sulfur content of BT, DBT, or DMDBT) was used as a model fuel. The reactions were carried out in a closed 50 mL double-necked glass flask equipped with a powerful magnetic stirrer (800 r/min) and immersed in a 50 °C water bath. In a standard run, catalyst (40 mg) was added to a mixture of model fuel (15 mL) and ethanol (10 mL) and then stirred at 50 °C for 30 min to reach thermal equilibrium. The catalytic reaction process is initiated by the addition of H_2O_2 (30 wt %, 135 μL) as oxidant with a H_2O_2/S molar ratio of 4:1.

The right amount of liquid in the *n*-octane phase was taken at different times under stirring and analyzed by an Agilent 7890A gas chromatography (GC) with an FID detector using a 30 m packed HP-5 column. The removal content of BT, DBT or DMDBT was calculated according to the equation $R = (1 - C_t/C_0) \times 100\%$, where C_0 and C_t stand for the initial concentration and the reaction concentration of BT, DBT or DMDBT in *n*-octane phase after *t* minutes, respectively.

In the recycling procedure, Ti_6tbbz_{10} was recovered by centrifugation, carefully washed and dried at the end of each reaction cycle. The recovered and treated catalysts were weighed and all experimental conditions, i.e., amount of reactants, were adjusted and maintained while performing successive reaction cycles.

1.10 Computational details

Density functional theory was employed to simulate Raman and FT-IR spectra of Ti_6tbbz_{10} clusters and Ti_6tbbz_{10} combined with H_2O_2 by different binding modes. The initial molecular structure model of Ti_6tbbz_{10} was constructed based on its single-crystal structure data. The molecular structure models of Ti_6tbbz_{10} combined with H_2O_2 were constructed based on the structure of Ti_6tbbz_{10} by incorporating two molecules of H_2O_2, owing to the centrosymmetric nature of Ti_6tbbz_{10}. The detailed structure was shown in Figure S22. All molecular structures were optimized using the PBE0[7] functional in conjunction with Grimme's DFT-D3(BJ)[8] semi-empirical dispersion correction and 6-31G (d) basis set. All stationary points were confirmed as minima through frequency calculations, ensuring that all frequencies were positive. The resonant frequency correction factor[9] of 0.9512 was applied to compensate for the non-resonant effects in the computation of Raman and FT-IR spectra. The interaction energy (ΔE) for the combination of TOCs and H_2O_2 was calculated using the following equation:

$$\Delta E = E(\text{TOCs} + \text{OOH}^-) - E(\text{TOCs}) - E(\text{OOH}^-)$$

where E (TOCs + OOH^-), E (TOCs) and E (OOH^-) represent the electronic energies of

TOCs combined with OOH^-, TOC, and OOH^-, respectively. A negative value of ΔE indicates an exothermic process, while more negative values imply a stronger binding affinity. All calculations were performed using Gaussian 16 programs.

2 The detailed structural information about Ti_{29} clusters

2.1 XRD patterns of Ti_{29} clusters prepared under different conditions

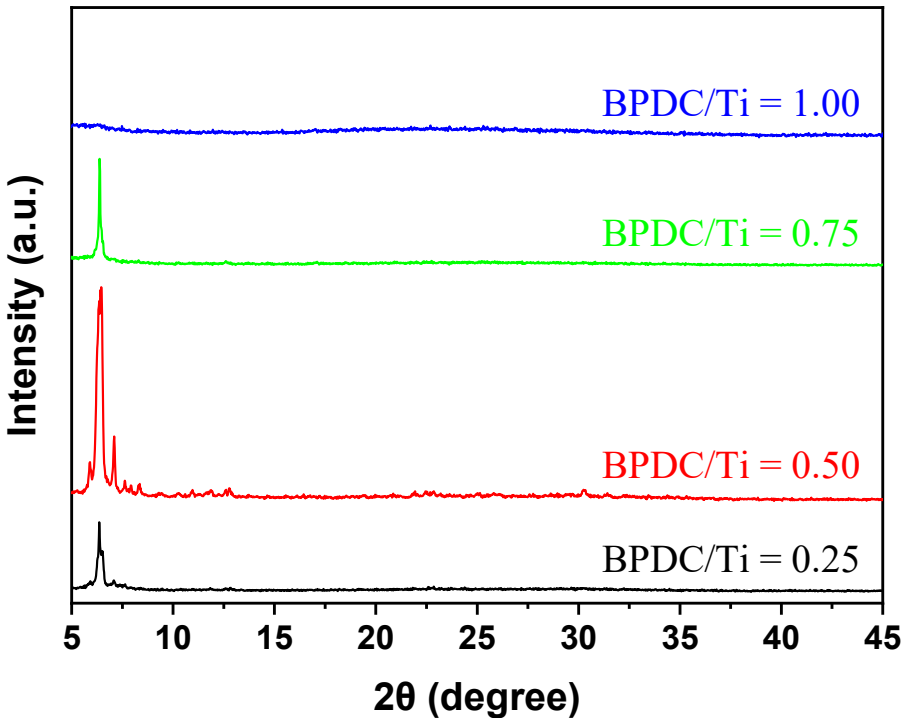

Figure S1. XRD patterns of Ti_{29} clusters prepared with different molar ratios of BPDC to $Ti(OEt)_4$.

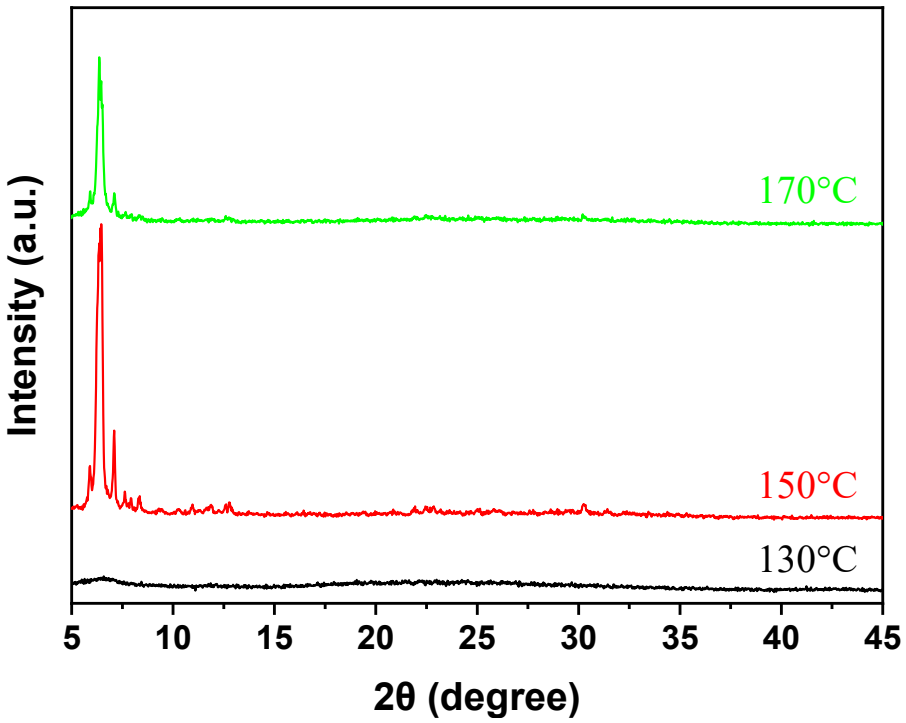

Figure S2. XRD patterns of Ti_{29} clusters prepared at different crystallization temperatures.

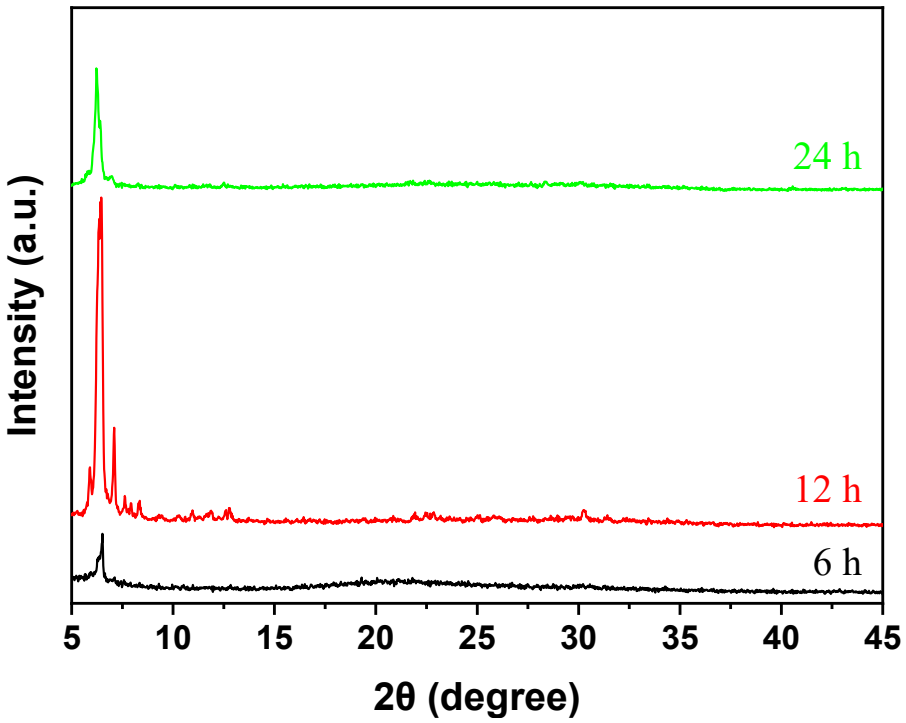

Figure S3. XRD patterns of Ti_{29} clusters prepared at different crytallization time.

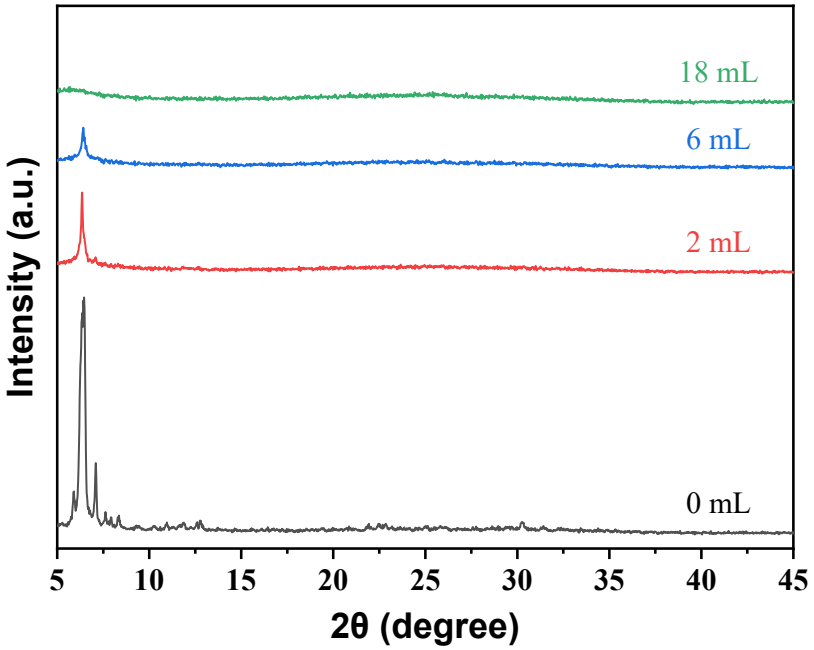

Figure S4. XRD patterns of Ti_{29} clusters prepared with different addition amount of ethanol.

2.2 Atomic arrangement of Ti_{29} clusters in different directions

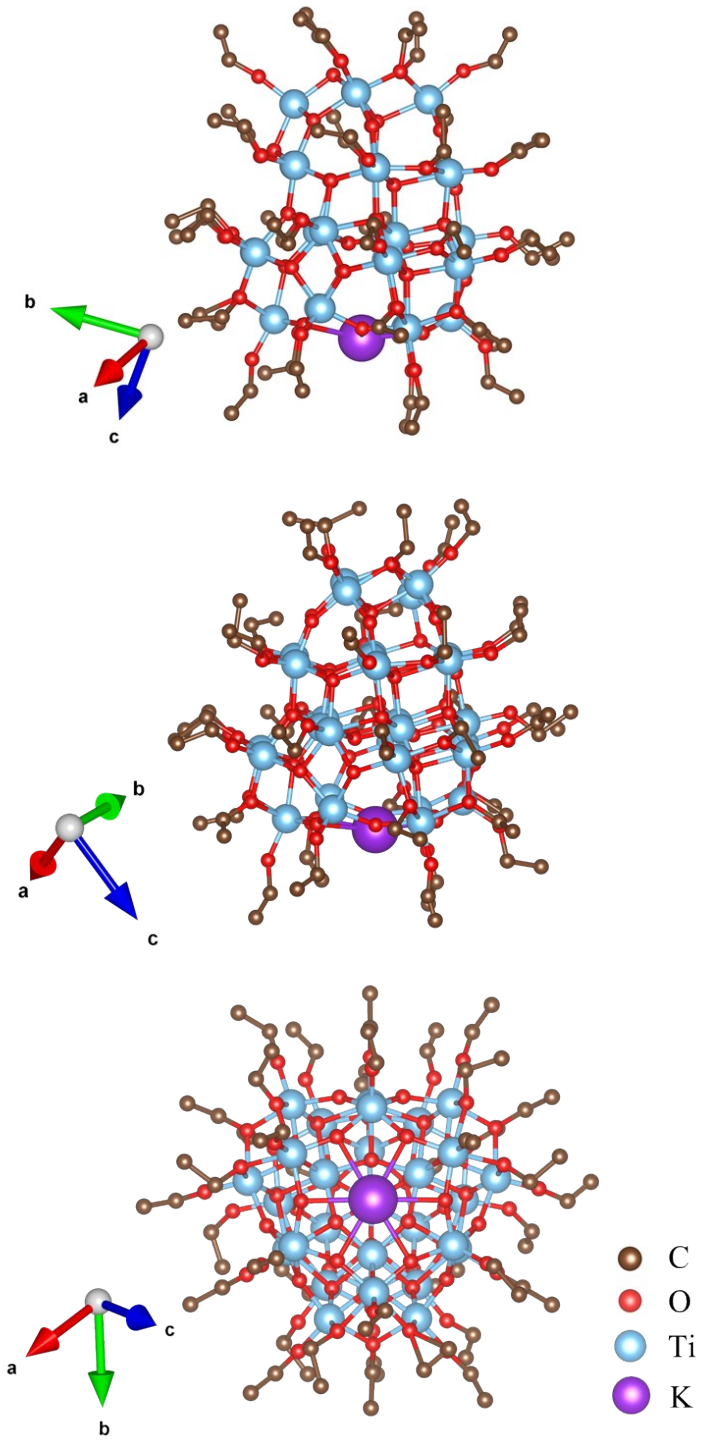

Figure S5. Atomic arrangement of Ti_{29} clusters in different directions. H atoms are omitted for clarity.

2.3 Comparison of XRD patterns of Ti_{29} clusters with $Ti_{28+\delta}NaO_{38}(OEt)_{39}$ clusters

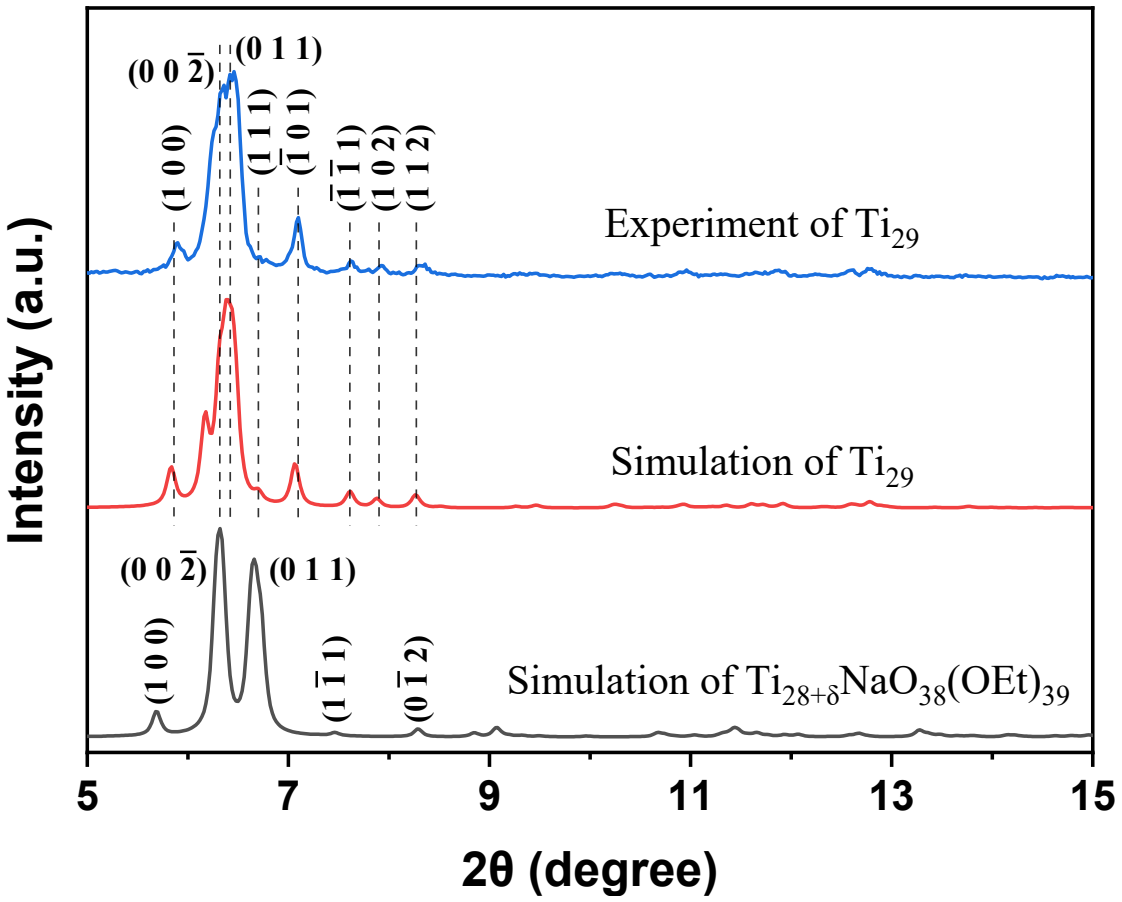

Figure S6. Comparison on XRD patterns of Ti_{29} clusters with reported $Ti28_{+\delta}NaO_{38}(OEt)_{39}$ clusters.

Ti_{29} clusters are different from the reported $Ti_{28+\delta}NaO_{38}(OEt)_{39}$ clusters[10] in terms of its physical phase structure, number of ligands and elemental composition although they possess similar structure.

2.4 FT-IR spectra of Ti_{29} clusters

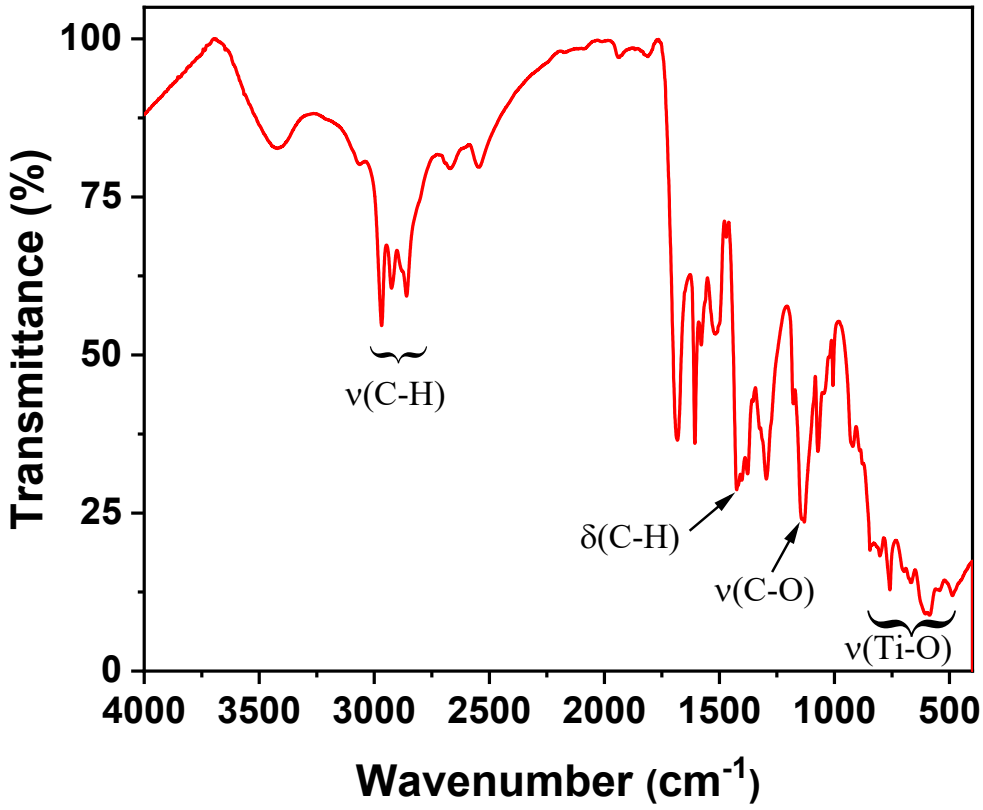

Figure S7. FT-IR spectroscopy of Ti_{29} clusters.

2.5 TGA curve of Ti_{29} clusters

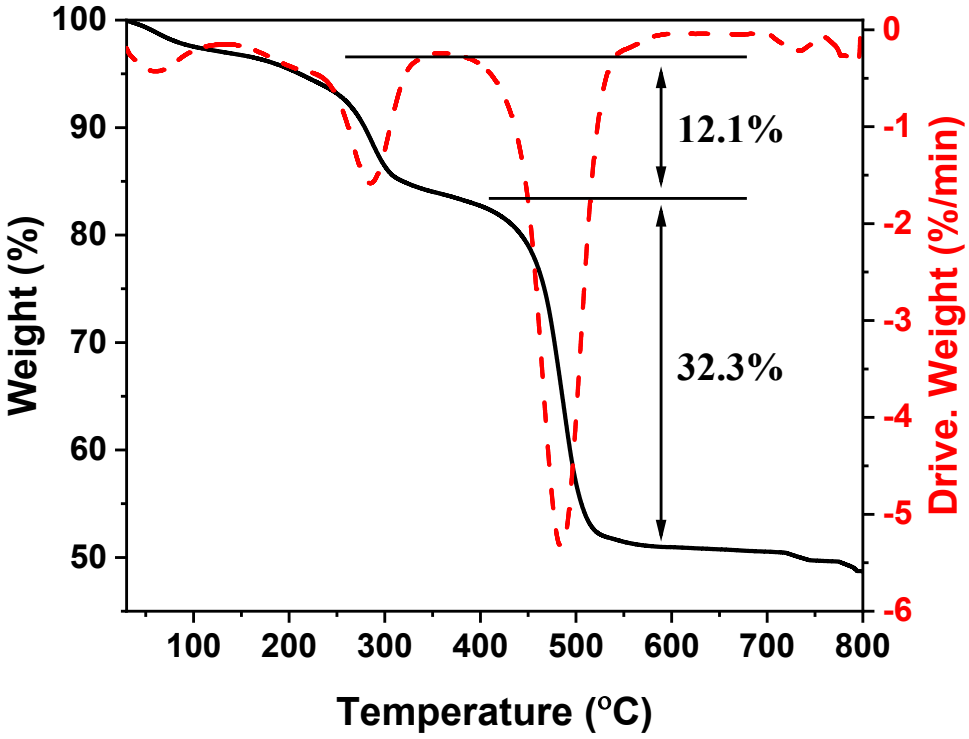

Figure S8. TGA curve of Ti_{29} clusters.

TGA curve of Ti_{29} clusters shows three distinct weight losses. The first loss before 150°C results from the physisorbed ethanol and water The second one between 200°C and 350°C is attributed to the removal of unstable ethoxylates in the structure of Ti_{29} clusters with a mass fraction of 12.1% corresponding to the molecular mass of 10 ethoxylates. The third one between 350°C and 550°C comes from the removal of relatively stable ethoxylates in Ti_{29} clusters with a mass fraction of 32.3% corresponding to the molecular mass of 28 ethoxylates. The total number of lost ethoxy groups is 38, which is the same as the number of ethoxy groups in Ti_{29} clusters.

2.6 Detection of K in Ti_{29} clusters

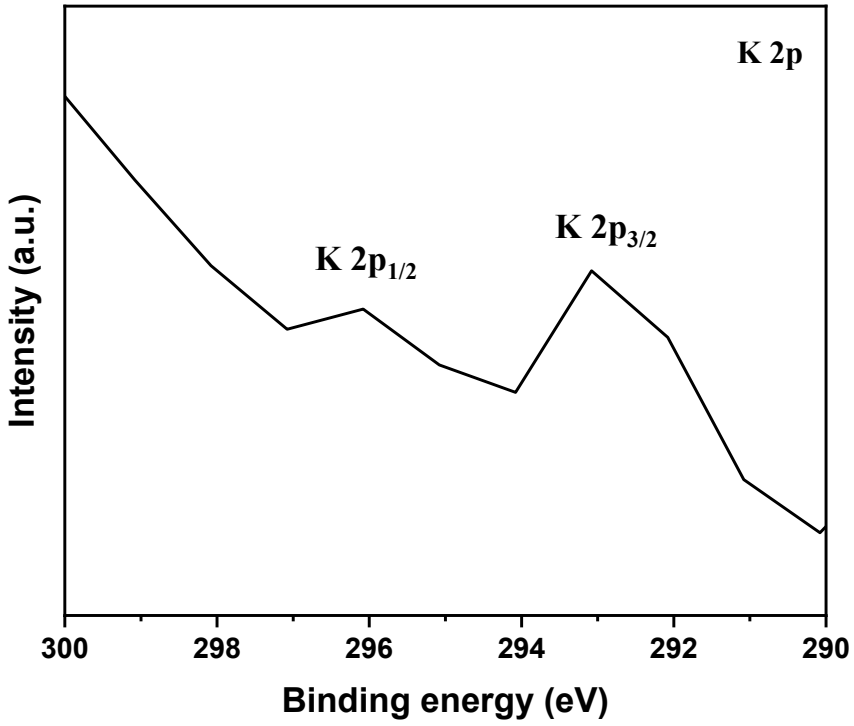

Figure S9. XPS spectrum for K 2p of Ti_{29} clusters.

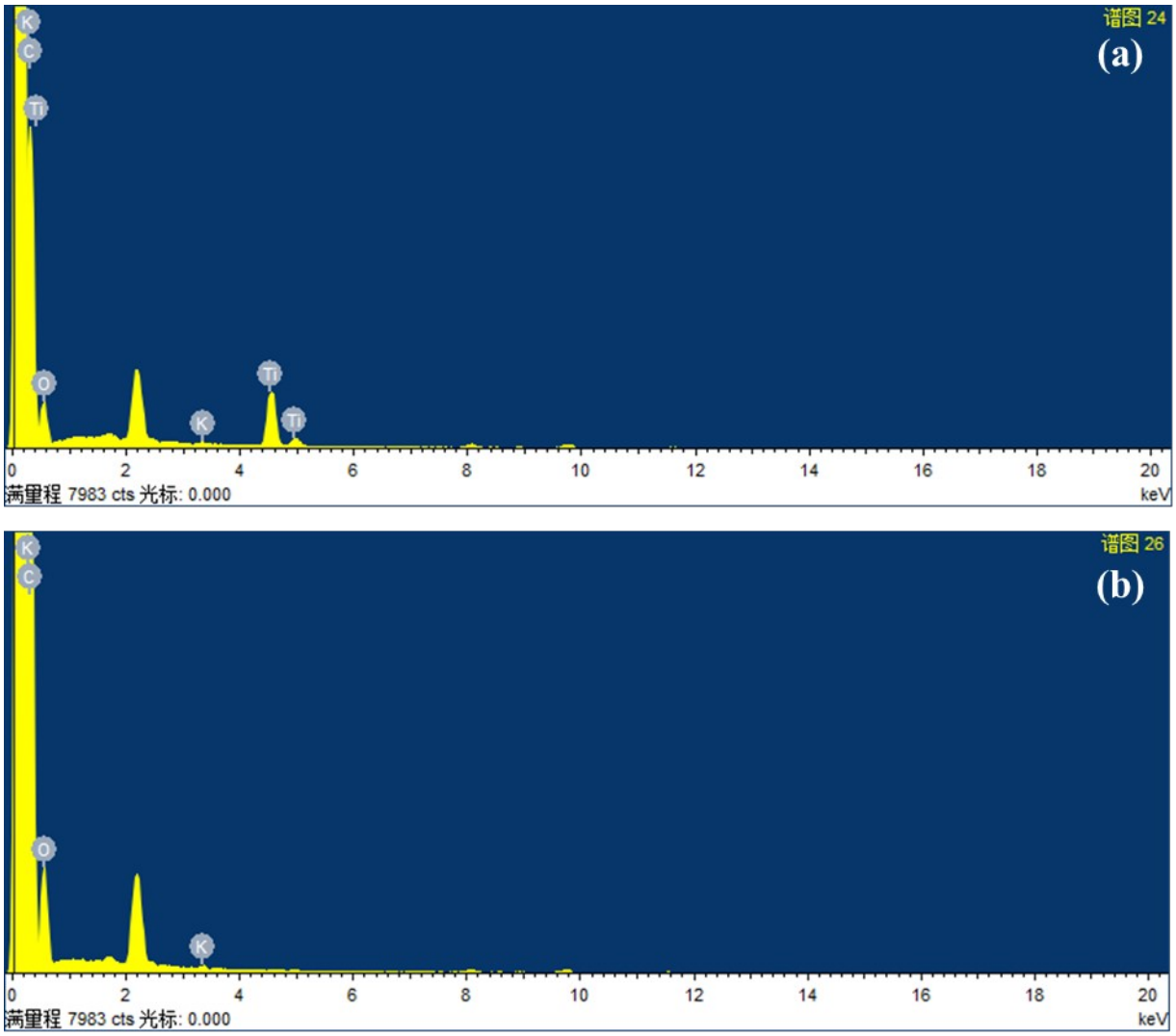

Figure S10. EDS patterns of Ti_{29} (a) clusters and BPDC (b).

The presence of the element K in Ti_{29} clusters may result from the impurities present in the BPDC ligand.

3 SEM images and elemental mapping of TOCs

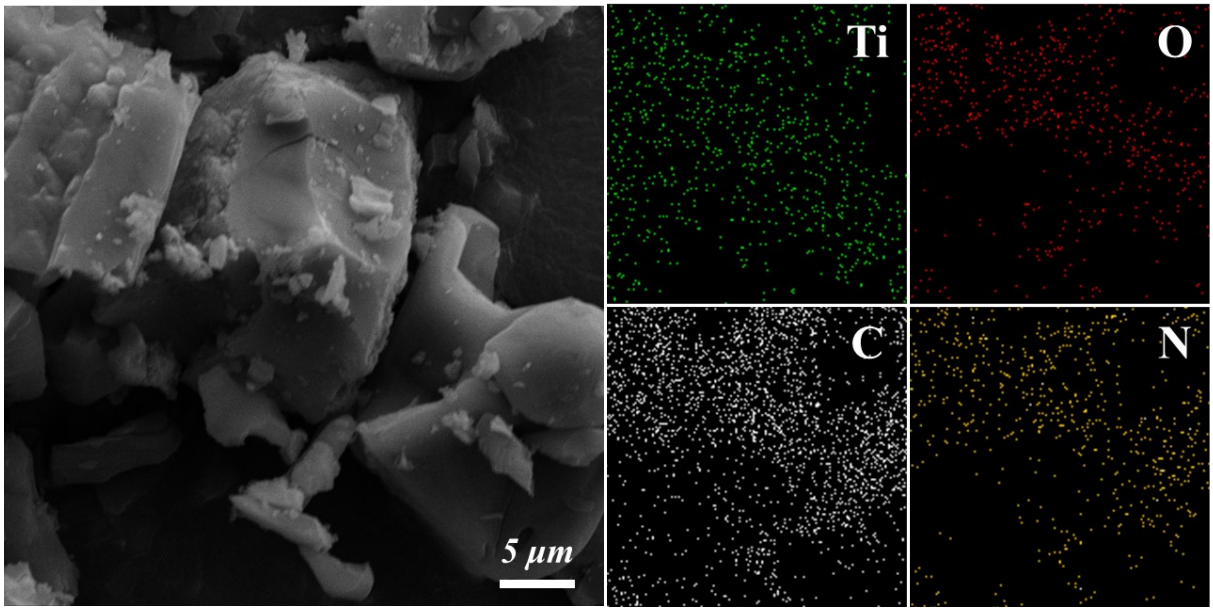

Figure S11. SEM image and elemental mapping of Ti_6abz_6 clusters.

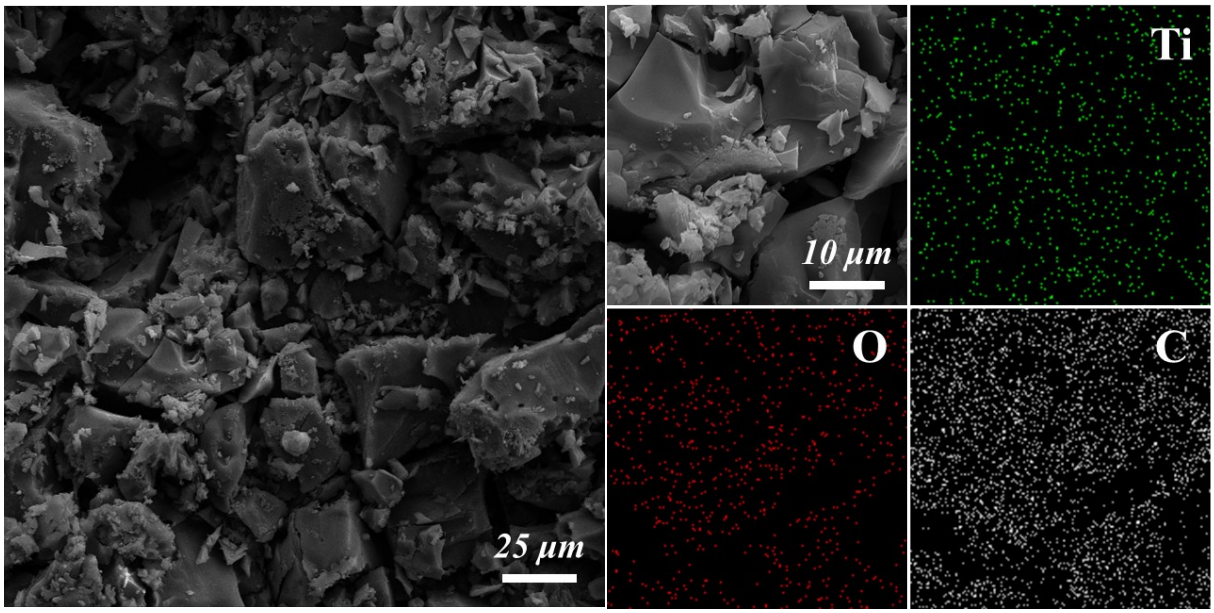

Figure S12. SEM image and elemental mapping of Ti_6tbbz_6 clusters.

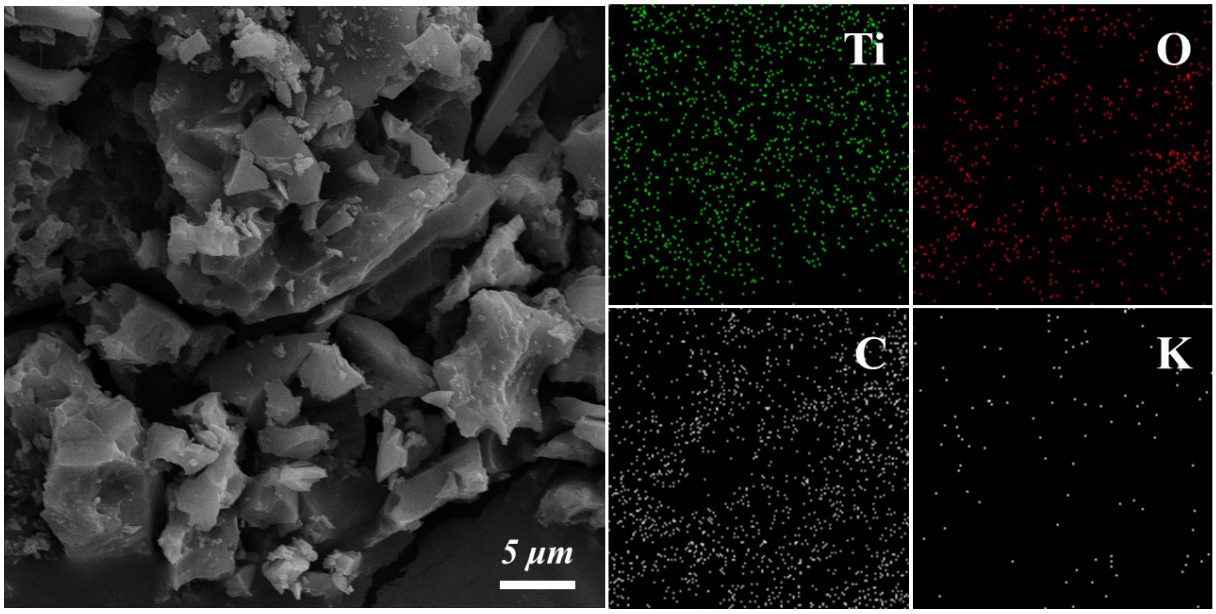

Figure S13. SEM image and elemental mapping of Ti_{29} clusters.

4 N_2-adsorption–desorption isotherms of TOCs

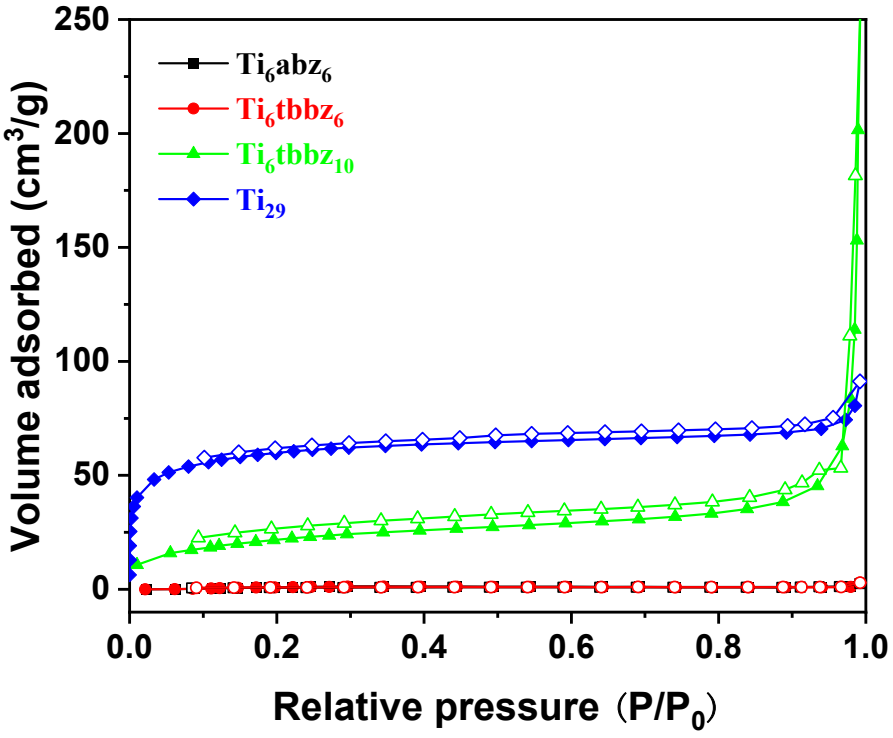

Figure S14. N_2 adsorption–desorption isotherms of different clusters.

5 XPS spectra of TOCs

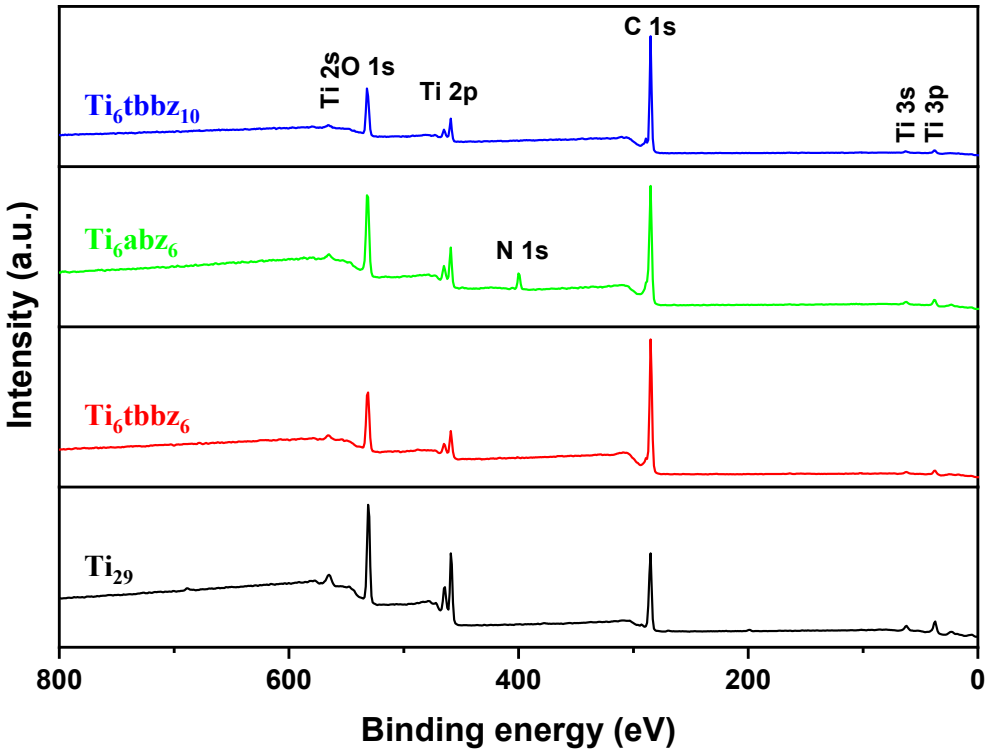

Figure S15. Survey spectra of different TOCs.

6 The hot-filtration test over Ti_6tbbz_{10} in the ODS reaction of BT

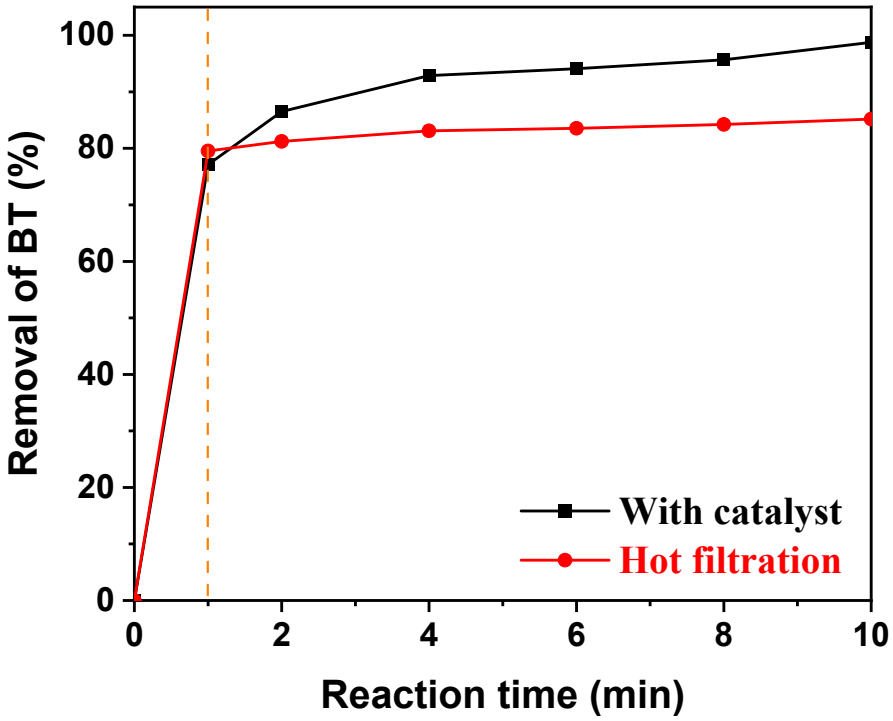

Figure S16. The hot-filtration test over Ti_6tbbz_{10} in the ODS reaction of BT. Reaction conditions: 40 mg catalyst, 15 mL model fuel oil, 10 mL ethanol, 1000 ppm sulfur content, reaction temperature of 50 °C, H_2O_2 as oxidant, O/S molar ratio of 4.

As shown, the removal of BT is almost inhibited when Ti_6tbbz_{10} catalyst is removed from the reaction system. The ICP analysis for the solution after reaction indicated a trace amount of Ti (6.5 ppm). These results demonstrated that Ti_6tbbz_{10} catalyst is a heterogeneous catalyst and can be reused.

7 Structural characterization of Ti_6tbbz_{10} before and after reaction

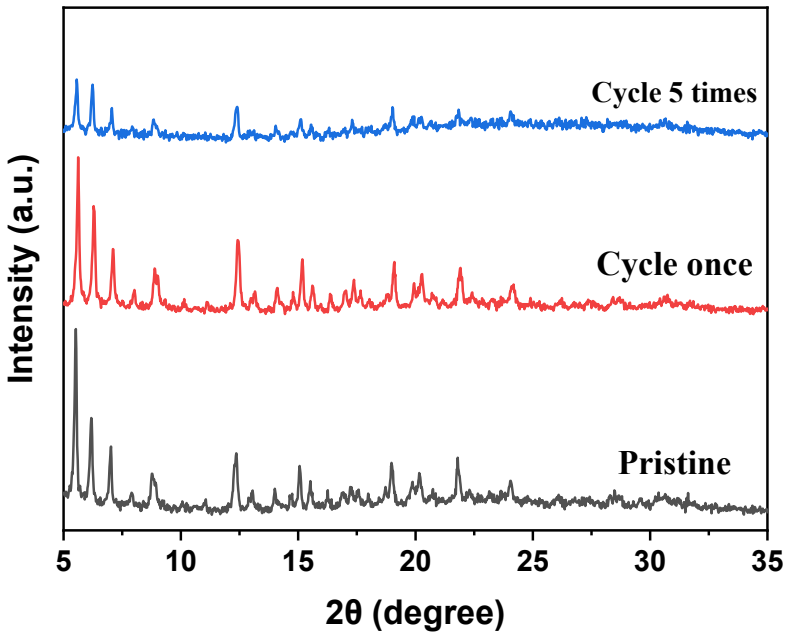

Figure S17. XRD patterns of Ti_6tbbz_{10} clusters before and after reaction.

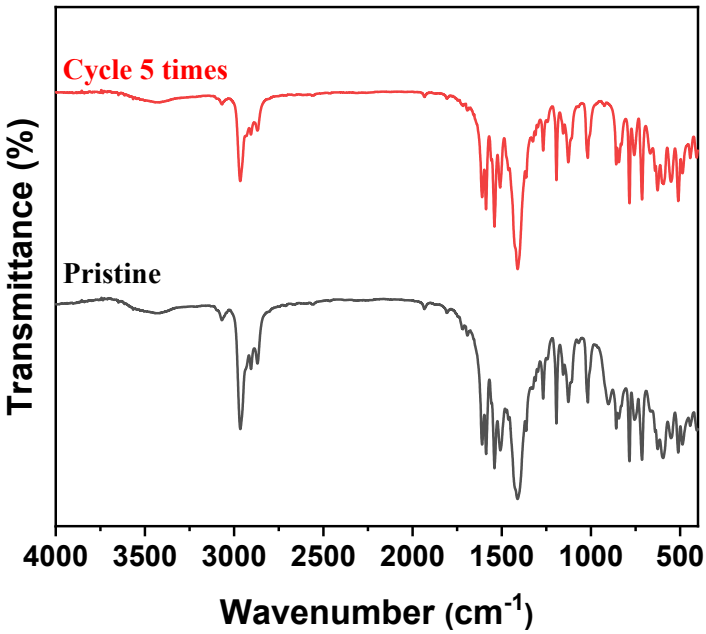

Figure S18. FT-IR spectra of Ti_6tbbz_{10} before and after reaction.

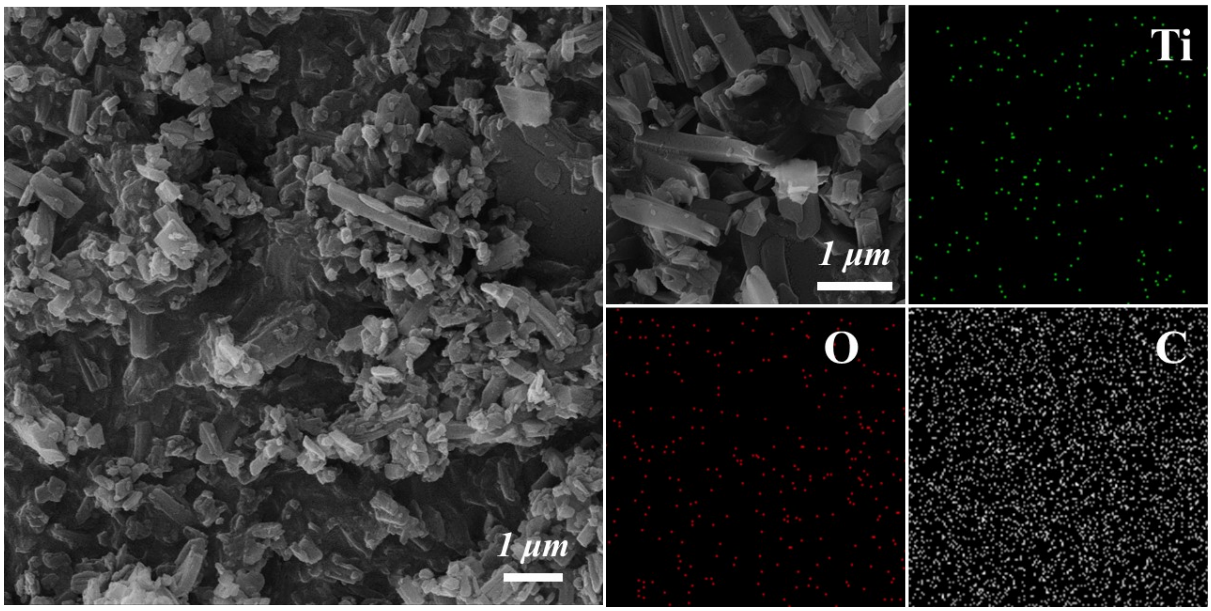

Figure S19. SEM images and elemental mapping of Ti_6tbbz_{10} clusters after one cycle.

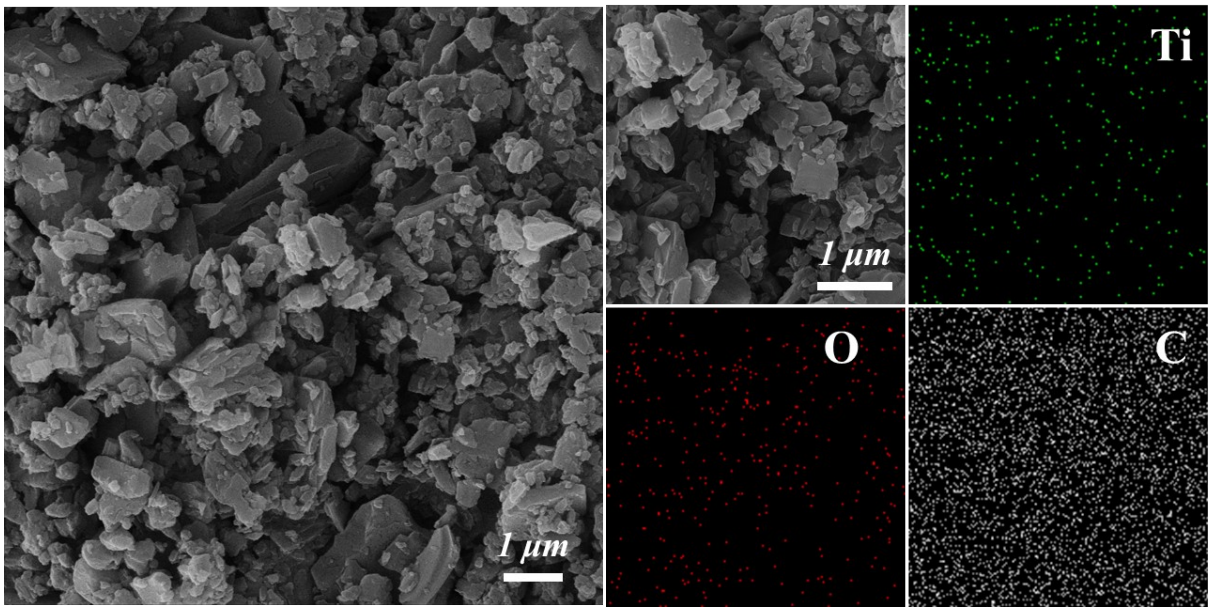

Figure S20. SEM images and elemental mapping of Ti_6tbbz_{10} clusters after five cycles.

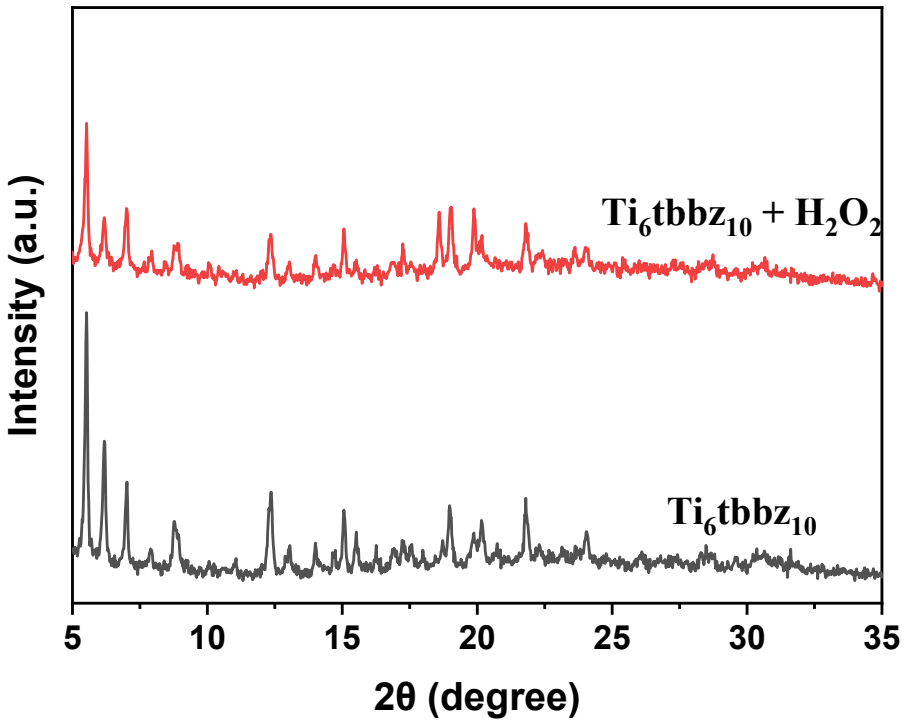

Figure S21. XRD patterns of Ti_6tbbz_{10} clusters before and after H_2O_2 treatment.

8 Different combination modes of Ti_6tbbz_{10} clusters and H_2O_2.

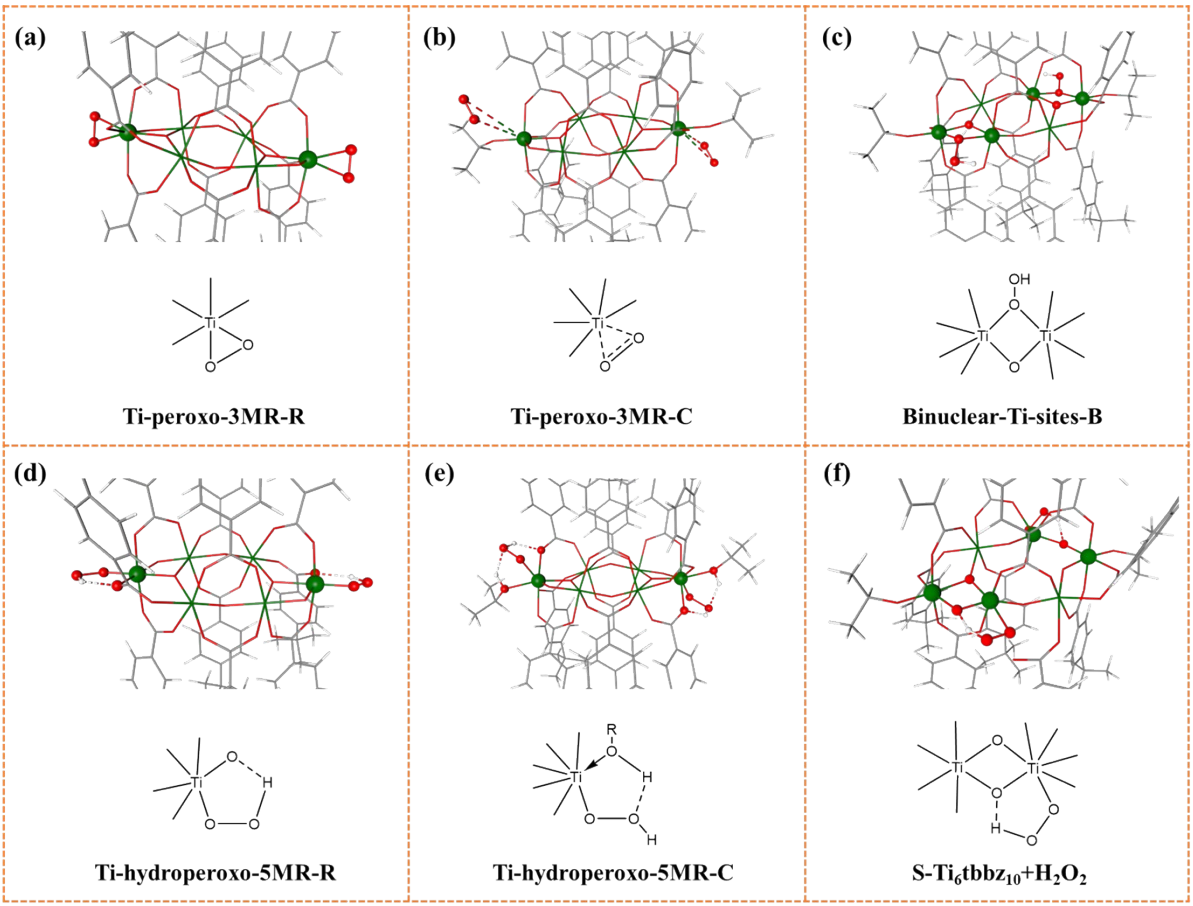

Figure S22. Different combination modes of Ti_6tbbz_{10} clusters and H_2O_2. (a) H_2O_2 replaces alkoxy to form Ti-peroxo-3MR-R. (b) H_2O_2 combines with Ti_6tbbz_{10} to form Ti-peroxo-3MR-C. (c) H_2O_2 is bridged at binuclear Ti sites. (d) H_2O_2 replaces alkoxy to form Ti-hydroperoxo-5MR-R. (e) H_2O_2 combines with the alkoxy group of Ti_6tbbz_{10} clusters to form Ti-hydroperoxo-5MR-C. (f) Ti-hydroperoxo-5MR structure formed by the interaction between binuclear titanium sites and H_2O_2. Symbols S, R, C, B and MR stand for simulation, replacement, combination, bridging and membered-ring, respectively. The part of Ti_6tbbz_{10} combined with H_2O_2 is highlighted. Ti (green), O (red).

9 Calculated Raman and FT-IR spectra of different Ti-hydroperoxo complexes

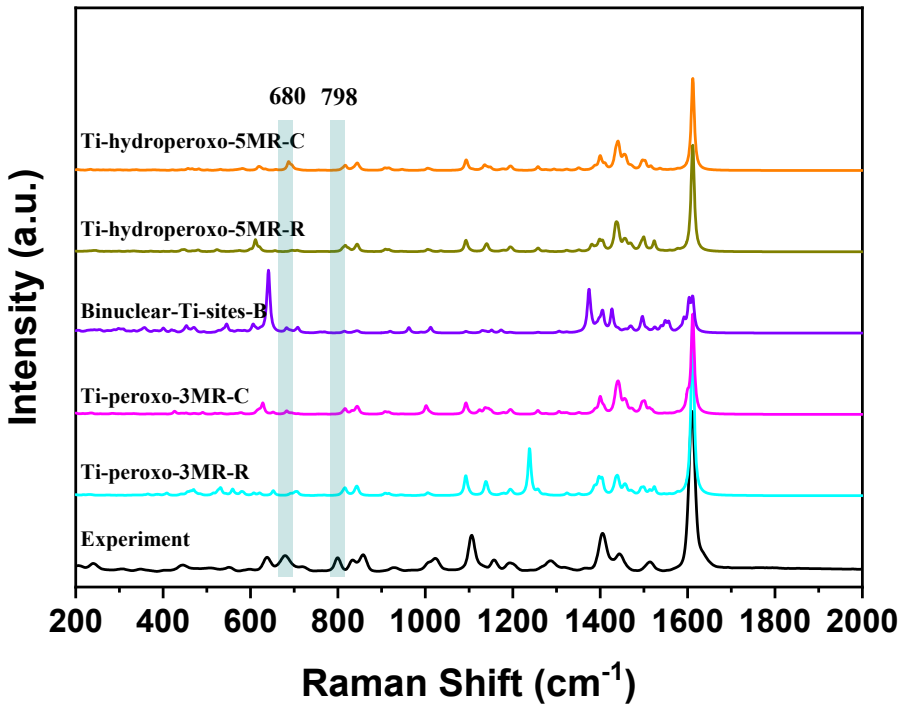

Figure S23. The Raman spectra of different Ti-hydroperoxo complexes obtained by experiment and calculations.

After H_2O_2 treatment, the Raman spectroscopy of Ti_6tbbz_{10} clusters showed obvious absorption peaks at 680 and 798 cm^{-1} corresponding to the stretching vibration of Ti-O bond. The oxygen in Ti-O bond comes from isopropoxy group and the binuclear titanium site, respectively. These results are consistent with Ti-hydroperoxo-5MR structure. It is noted that no absorption peaks belonging to the binding modes of Ti-peroxo-3MR-R, Ti-peroxo-3MR-C, Binuclear-Ti-sites-B, Ti-hydroperoxo-5MR-R and Ti-hydroperoxo-5MR-C were observed in the simulated Raman spectra.

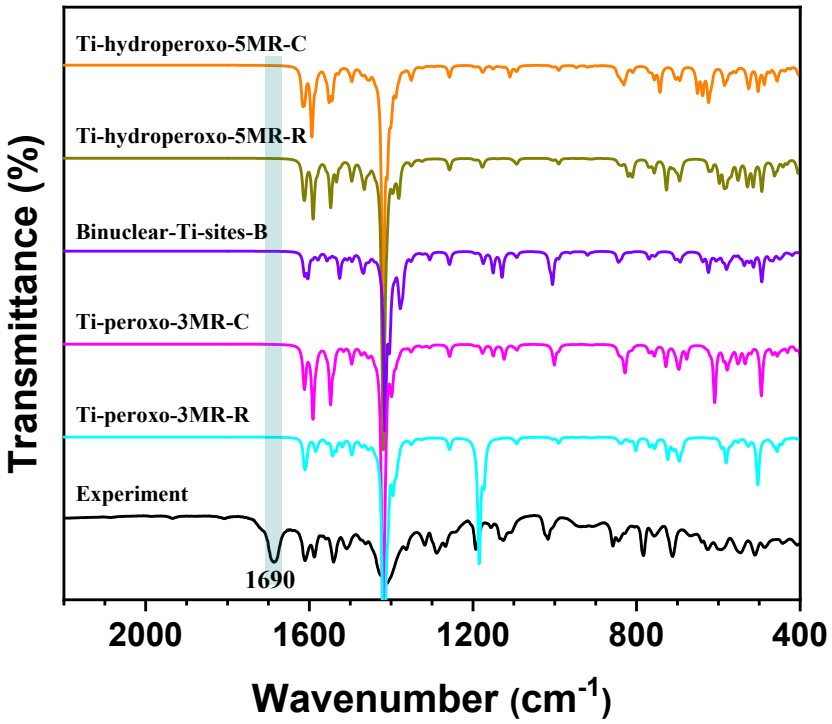

Figure S24. The FT-IR spectra of different Ti-hydroperoxo complexes obtained by experiment and calculations.

The FT-IR spectroscopy of Ti_6tbbz_{10} clusters binding with H_2O_2 showed an absorption peak at 1690 cm^{-1} corresponding to the stretching vibration of the C=O bond associated with the monodentate bridging coordination mode in the carboxylic acid ligand. Notably, this peak was present in the combined mode of Ti-hydroperoxo-5MR. No absorption peak corresponding to Ti-peroxo-3MR-R, Ti-peroxo-3MR-C, Binuclear-Ti-sites-B, Ti-hydroperoxo-5MR-R, and Ti-hydroperoxo-5MR-C were observed at 1690 cm^{-1} in the simulated FT-IR spectra.

10 ESI-MS of Ti_6abz_6 clusters before and after H_2O_2 treatment

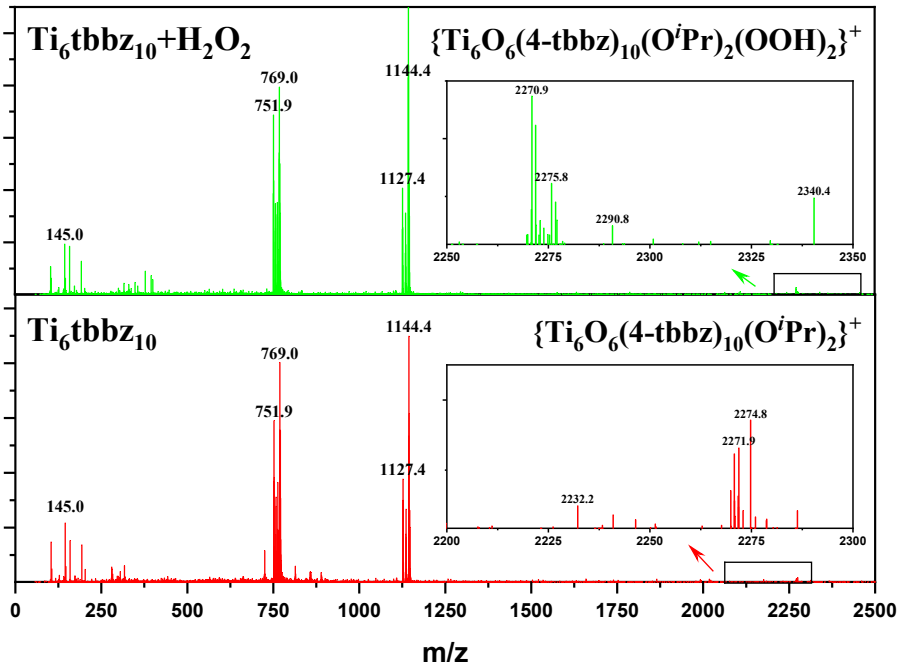

Figure S25. ESI-MS of Ti_6tbbz_{10} before and after adding H_2O_2. Insert show the locally enlarged information. 4-tbbz = 4-tert-butylbenzoic acid, O^iPr = isopropanol.

As shown in Figure S24, before adding H_2O_2 the peak at 2274.8 in the locally amplified mass spectrum belongs to $\{Ti_6O_6(4\text{-tbbz})_{10}(O^iPr)_2\}^+$ (calcd m/z = 2274.6), which corresponds to Ti_6tbbz_{10} clusters combined with one H^+. After the addition of H_2O_2 into the above solution, the peak at 2340.4 is observed, which is attributed to $\{Ti_6O_6(4\text{-tbbz})_{10}(O^iPr)_2(OOH)_2\}^+$ (calcd m/z = 2340.6) corresponding to Ti_6tbbz_{10} combined with two -OOH and one H^+. These results are consistent with the structure of Ti-hydroperoxo-5MR.

11 Oxidation of Ti_6abz_6 clusters after H_2O_2 treatment

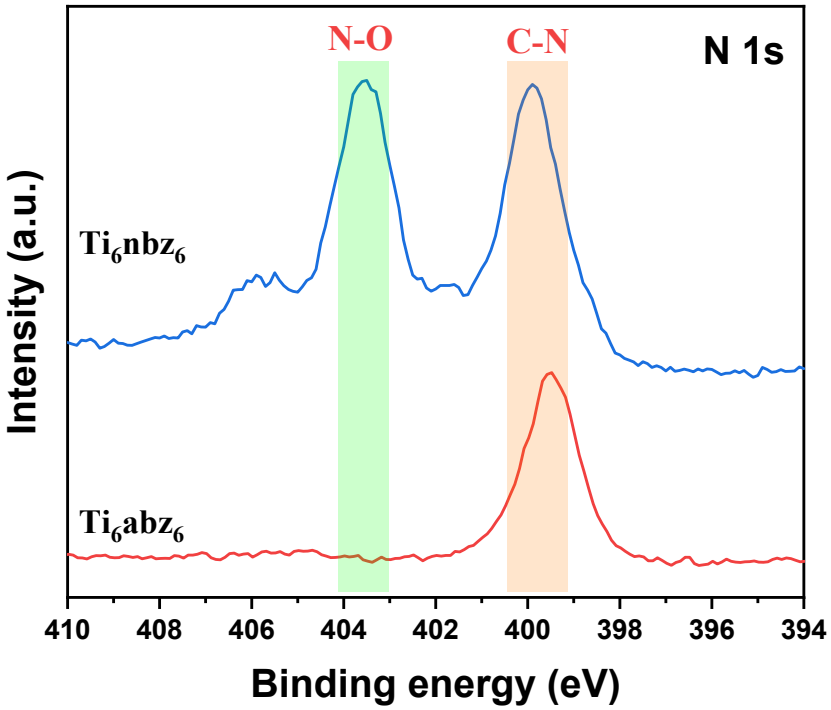

Figure S26. N 1s high-resolution XPS spectra of Ti_6abz_6 and Ti_6nbz_6 (Ti_6abz_6 oxidized by H_2O_2) clusters..

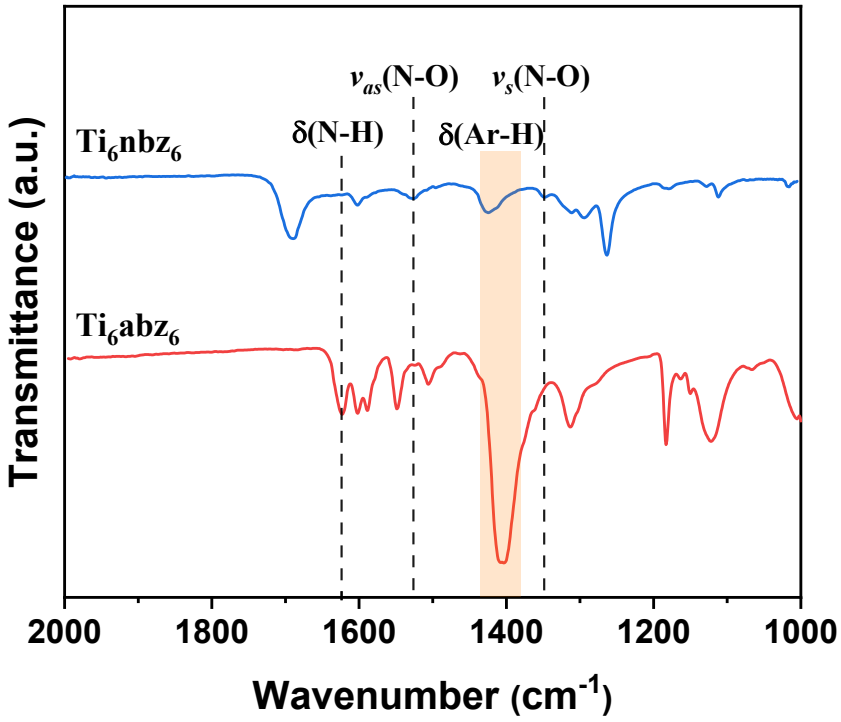

Figure S27. FT-IR spectra of Ti_6abz_6 and Ti_6nbz_6 clusters.

12 Detection of hydroxyl radicals in oxidative desulfurization processes

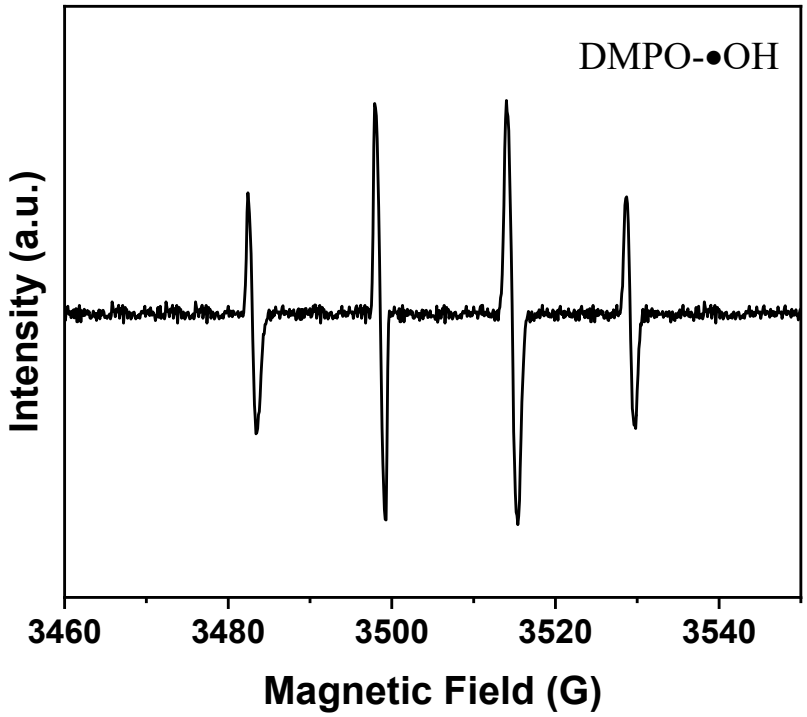

Figure S28. EPR spectrum of 10 mg Ti_6tbbz_{10} clusters, 2.5 mL H_2O, 50 μL H_2O_2 and 50 μL DMPO.

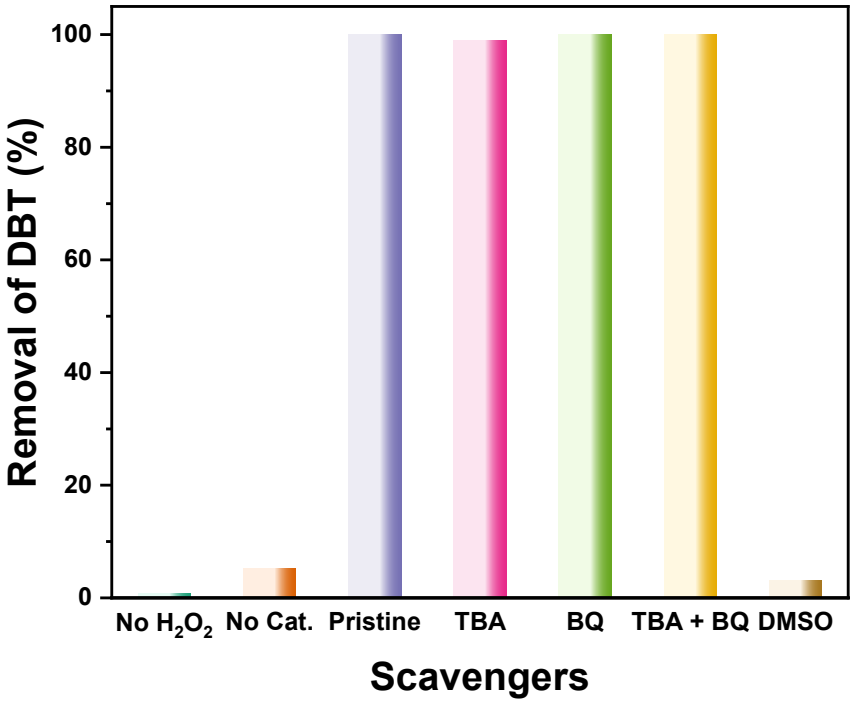

Figure S29. Quenching experiments over Ti_6tbbz_{10} clusters in the ODS reaction of DBT. Reaction conditions: catalyst amount (40 mg), model oil (15 mL), ethanol (10 mL), sulfur content (1000 ppm), oxidant (H_2O_2), O/S molar ratio (4:1), reaction temperature (50 °C), reaction time (1 min).

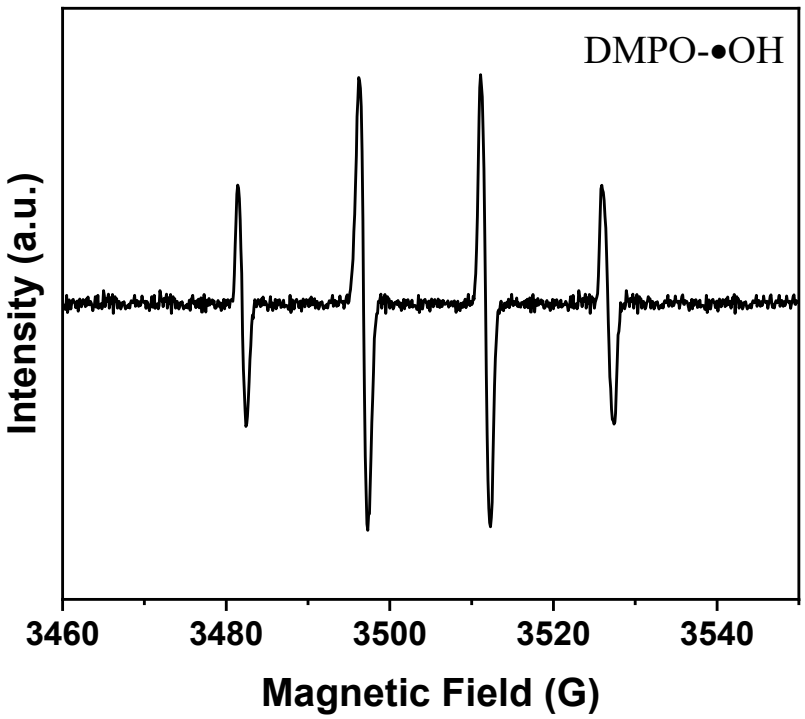

Figure S30. EPR spectrum of 10 mg Ti_6tbbz_{10} clusters, 2.5 mL absolute ethanol, 50 μL H_2O_2 and 50 μL DMPO.

13 Optimized reaction pathways for the DBT oxidation process

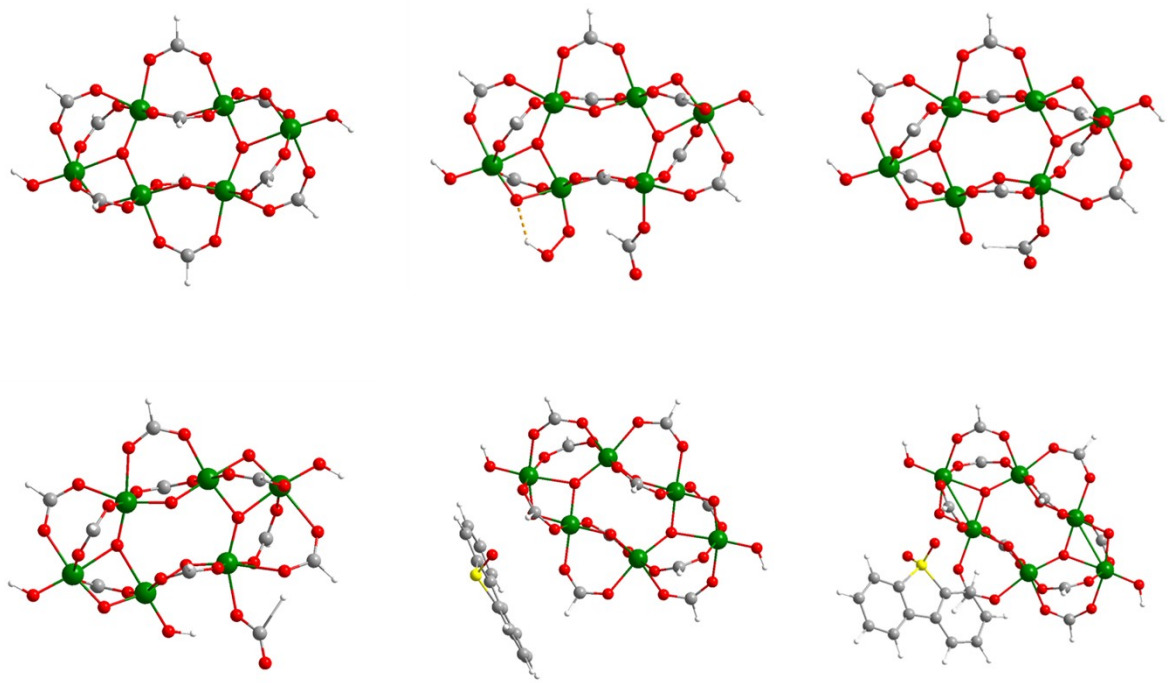

Figure S31. Optimized reaction pathways for the oxidation process of DBT at the PBE0-D3 / 6-31G (d) level. 4-tert-butylbenzoic acid substituted with formic acid and isopropoxy substituted with hydroxyl to simplify the calculations.

14 Comparison on the yield of products prepared by solid-phase synthesis and solvothermal methods

Figure S32. Yields of Ti_6tbbz_{10} clusters synthesized with autoclaves of the same size by solid-phase (left) and solvothermal method (right) .

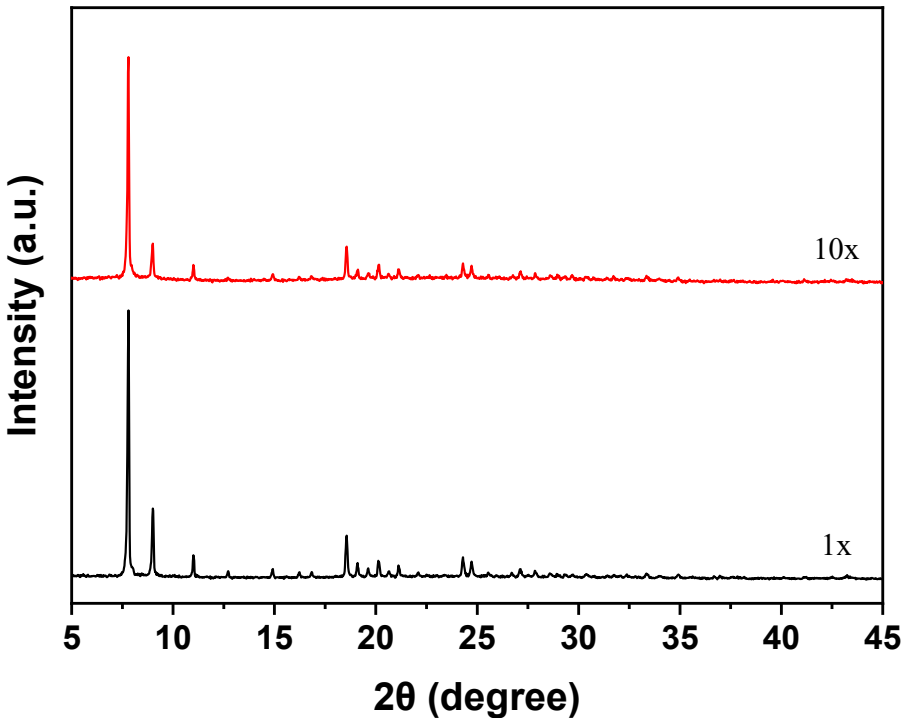

Figure S33. XRD patterns of Ti_6abz_6 clusters synthesized at small and large scales.

15 Ti_6abz_6 clusters as precursors for the synthesis of MIL-125(Ti) and MUV-10(Ti, Mn)

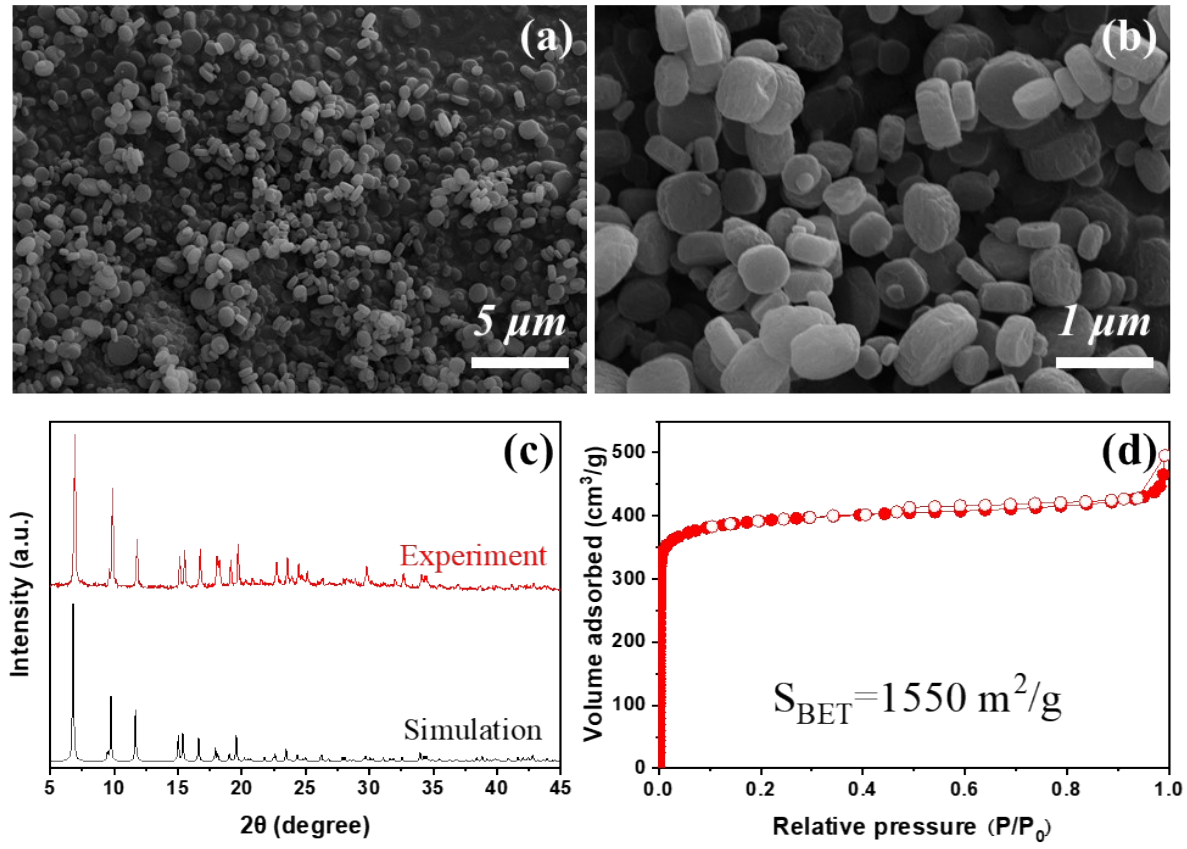

Figure S34. SEM images (a, b), PXRD patterns (c) and N_2 adsorption–desorption isotherms (d) of MIL-125(Ti) synthesized with Ti_6abz_6 clusters as precursors.

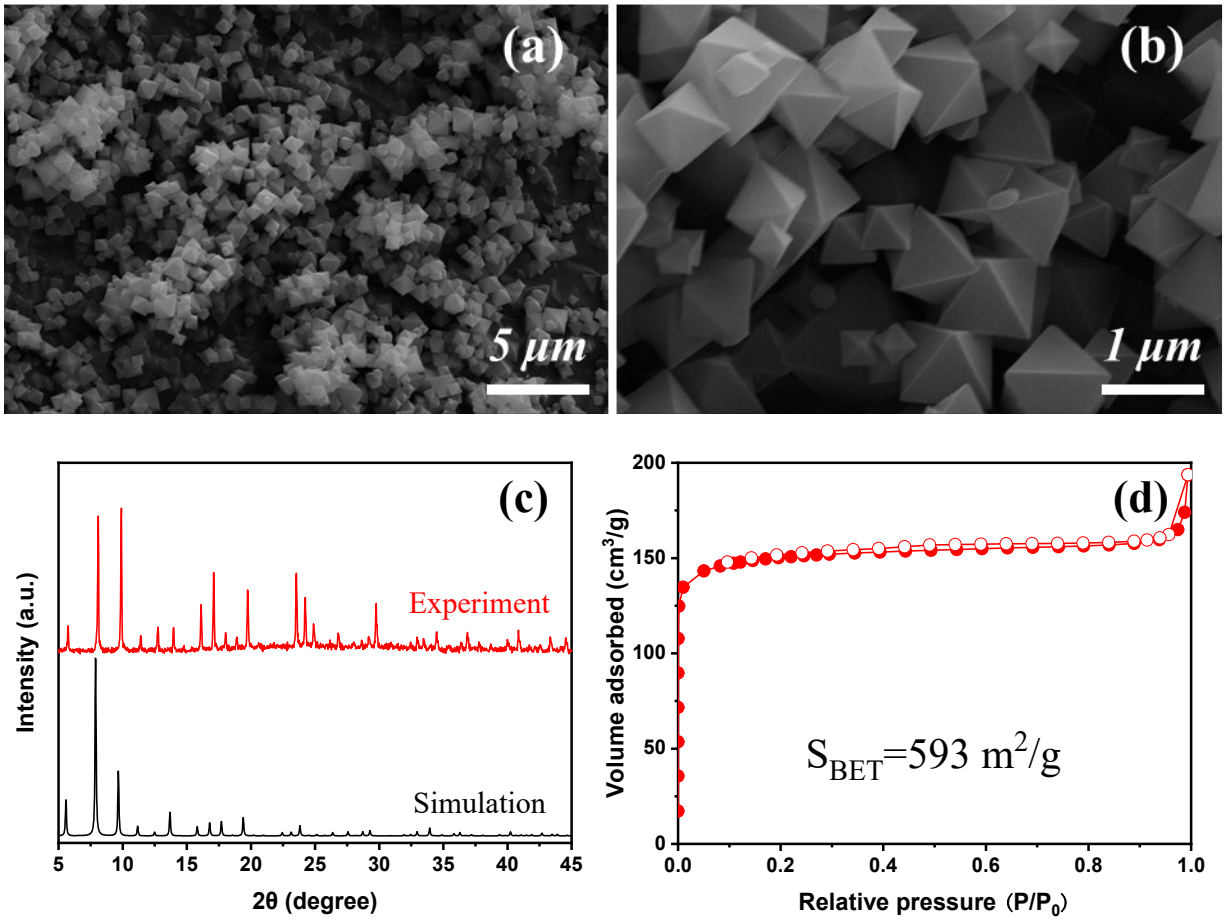

Figure S35. SEM images (a, b), PXRD patterns (c) and N_2 adsorption-desorption isotherms (d) of MUV-10(Ti, Mn) synthesized with Ti_6abz_6 clusters as precursors.

16 Crystal structure data of Ti_{29} clusters

Table S1. The summary of crystal data and structure refinement for Ti_{29} clusters.

Compounds	Ti_{29}
CCDC No	2286846
Formula	$Ti_{29}KO_{77}C_{76}H_{190}$
FW	3764.47
T (K)	298.3
λ (Å)	0.71073
Crystal system	Triclinic
Space group	$P\bar{1}$
a (Å)	16.5381(9)
b (Å)	17.0084(9)
c (Å)	28.4386(16)
α (deg)	85.261(3)
β (deg)	79.664(3)
γ (deg)	68.022(2)
V ($Å^3$)	7296.6(7)
Z	2
ρ_{calc} (g/cm^3)	1.713
μ (mm^{-1})	1.603
F(000)	3838
Crystal size (mm^3)	0.20 × 0.15 × 0.08
2θ range (deg)	2.6 ~ 50.0
h, k, l ranges	-19/19, -20/20, -33/33
Reflections collected	134312
Independent (R_{int})	25683 (0.0799)
Data/restraints/parameters	25683/148/1345
GOF on F^2	1.044
R_1, wR_2 [$I >= 2\sigma(I)$]	0.0697, 0.1844
R_1, wR_2 [all data]	0.1019, 0.2087
Largest diff. peak/hole ($e/Å^3$)	1.07/-1.06

17 Element content in different TOCs

Table S2. Element content in Ti_{29} clusters.

	Ti (at %)	O (at %)	C (at %)	K (at %)
Theoretical value	15.8	42.2	41.5	0.5
XPS	12.7	32.8	54.4	0.1
EDS	9.8	43.1	46.8	0.3

Table S3. Element content in Ti_6tbbz_6 clusters.

	Ti (at %)	O (at %)	C (at %)
Theoretical value	5.3	21.0	73.7
XPS	4.5	18.1	77.4
EDS	4.0	26.2	69.8

Table S4. Element content in Ti_6abz_6 clusters.

	Ti (at %)	O (at %)	C (at %)	N (at %)
Theoretical value	6.2	25.0	62.5	6.3
XPS	5.5	21.7	66.3	6.5
EDS	4.7	32.3	41.0	22.0

Table S5. Element content of Ti_6tbbz_{10} clusters.

	Ti (at %)	O (at %)	C (at %)
Theoretical value	4.0	18.7	77.3
XPS	4.4	17.9	77.7
EDS	3.9	28.6	67.5

18 Nitrogen sorption data for different TOCs

Table S6. Nitrogen sorption data for different TOCs.

Entry	Clusters	Surface area ($m^2\ g^{-1}$)	Pore volume ($cm^3\ g^{-1}$)	Average pore size (nm)
1	Ti_{29}	213	0.136	2.56
2	Ti_6tbbz_6	5	0.004	3.28
3	Ti_6abz_6	10	0.004	1.48
4	Ti_6tbbz_{10}	80	0.325	16.30

19 Proportion of carboxylic acid ligands in different TOCs

Table S7. Proportion of carboxylic acid ligands and binding energy of the Ti $2p_{3/2}$ peaks in different clusters.

Entry	Clusters	N_1[a]	N_2[b]	N_1/N_2	Ti $2p_{3/2}$ (eV)
1	Ti_{29}	0	38	0	458.66
2	Ti_6tbbz_6	6	12	0.50	458.78
3	Ti_6abz_6	6	12	0.50	458.95
4	Ti_6tbbz_{10}	10	12	0.83	459.00

[a] N_1 represents the number of carboxylic acid ligands in each cluster.

[b] N_2 represents the total number of ligands in each cluster.

20 Comparison of catalytic activities in the ODS reaction of DBT

Table S8. Comparison of catalytic activities over representative Ti-containing catalysts in the ODS reaction of DBT.

Catalysts	Dosage of catalyst (mg)	Metal content (wt %)	Sulfur content (ppm)	Oxidant	O/S molar ratio	Temp. (°C)	TOF[a] (h^{-1})	Activity[b] (mmol h^{-1} g^{-1})	Ref.
Ti_{32}-BTA	50	22.3	200	H_2O_2	6	60	0.6	2.7	11
MIL-125(Ti)	17.3	24.4	500	TBHP	10	80	5.6	21.4	12
MIL-125-CA-5	100	24.4	1000	H_2O_2	8	60	4.4	22.4	13
COK-47s	32.5	22.1	3594	TBHP	2.5	60	8.0	36.9	14
Hier-NTU-9	20	26.9	1000	TBHP	4	80	0.3	1.9	15
Ti-BDC-180	50	23.0	1000	H_2O_2	6	60	7.8	37.2	16
Ti-BDC-A	30	26.8	500	CHP	6	50	33.2	185.8	17
H-TiNTs	100	59.9	320	H_2O_2	4	40	0.4	5.2	18
UiO-66(Zr,Ti)	50	5.1	1000	H_2O_2	6	60	0.7	2.9	19
10%MIL-101(Cr)-TiO_2	100	33.0	100	CHP	6	60	0.9	6.1	20
M-TS-1	120	0.6	200	CHP	15	80	6.3	0.8	21
Ti-MCM-41S	25	1.3	1740	TBHP	2.5	80	18.2	4.8	22
Ti-SBA-2	30	5.5	500	TBHP	3	40	48.6	56.1	23
Ti-B-M-DA	50	5.5	1000	TBHP	6	60	58.8	65.9	24
TS-1	55	0.9	500	TBHP	2	60	232.2	45.6	25
Meso-TS-6H	20	3.2	1000	TBHP	2	60	480.7	316.4	26
Ti_6tbbz_{10}	10	12.6	1000	H_2O_2	4	50	729.0	1918.8	This work

[a] TOF = (mole number of converted sulfur) / (mole of active species in catalyst × reaction time (h)),

[b] Activity = (millimole number of converted DBT) / (reaction time (h) × dosage of catalyst (g)).

Table S9. Comparison of catalytic activities over representative catalysts in the ODS reaction of DBT.

Catalysts	Dosage of catalyst (mg)	Active species and content (wt %)	Sulfur content (ppm)	Oxidant	O/S molar ratio	Temp. (°C)	TOF[a] (h^{-1})	Activity[b] (mmol h^{-1} g^{-1})	Ref.
Mo-INFs	1000	Mo/2	500	H_2O_2	5	60	0.7	0.1	[27]
Mo_2N/rGO-A	20	Mo/20.9	1000	H_2O_2	10	60	28.1	61.3	[28]
MoO_3@NPC	5	Mo/1.5	200	H_2O_2	3	60	96.2	20.6	[29]
$MoWP_2$/C	3	MoW/19.6	500	H_2O_2	4	60	105.4	87.9	[30]
Fe_3O_4@CTS@PMoW	50	MoW/-	500	H_2O_2	5	60	-	1.0	[31]
PW_{12}@UiO-67(Zr)	50	W/28	1000	H_2O_2	13	70	21.5	5.3	[32]
30W/HNT/M	60	W/0.5	500	H_2O_2	5	60	34.5	2.9	[33]
Meso-SiO_2	25	W/15.3	500	H_2O_2	4	60	15.7	13.2	[34]
Co@C-P5	10	Co/1.1[c]	1000	H_2O_2	7.5	60	104.0	158.2	[35]
CrN@C-6	20	Cr/4.5	250	H_2O_2	10	60	32.5	9.9	[36]
UiO-66(Zr)	15	Zr/33.1	500	H_2O_2	45	50	0.3	1.1	[37]
Ti_6tbbz_{10}	10	Ti/12.6	1000	H_2O_2	4	50	729.0	1918.8	This work

[a] TOF = (mole number of converted sulfur) / (mole of active species in catalyst × reaction time (h)),

[b] Activity = (millimole number of converted DBT) / (reaction time (h) × dosage of catalyst (g)).

[c] Atomic percentage.

21 Catalytic performance of Ti_6tbbz_{10} clusters in the other oxidation reactions

Table S10. Catalytic performance of Ti_6tbbz_{10} in the other oxidation reactions.

Substrate	Time	Temperature	Catalyst	Oxidant	Solvent	Conversion[a]
Benzyl alcohol (0.25 mmol)	90 min	60°C	50 mg	H_2O_2 (1 mmol)	Ethanol (10 mL)	31.2%
Cyclohexene (0.25 mmol)	90 min	60°C	50 mg	H_2O_2 (1 mmol)	Ethanol (10 mL)	47.4%

[a] Based on substrate.

22 Space-time yields of TOCs

Table S11. Space-time yields of different TOCs prepared by different methods.

	Yields (g)	Formula weight	Space-time yields ($kg \cdot m^{-3} \cdot h^{-1}$)	
			Reference	This work
Ti_{29}	0.5982	3764.47	-	8.31
Ti_6abz_6	0.7629	1554.68	0.16[1]	14.54
Ti_6tbbz_6	0.2324	1801.20	0.15[2]	3.48
Ti_6tbbz_{10}	1.134	2273.71	0.18[2]	18.84

23 References

1 K. Hong and H. Chun, *Inorg. Chem.*, 2013, **52**, 9705–9707.
2 K. Hong, W. Bak and H. Chun, *Inorg. Chem.*, 2014, **53**, 7288–7293.
3 M. Dan-Hardi, C. Serre, T. Frot, L. Rozes, G. Maurin, C. Sanchez and G. Férey, *J. Am. Chem. Soc.*, 2009, **131**, 10857–10859.
4 J. Castells-Gil, N. M. Padial, N. Almora-Barrios, J. Albero, A. R. Ruiz-Salvador, J. González-Platas, H. García and C. Martí-Gastaldo, *Angew. Chem. Int. Ed.*, 2018, **57**, 8453–8457.
5 D. Kratzert, J. J. Holstein and I. Krossing, *J. Appl. Crystallogr.*, 2015, **48**, 933–938.
6 O. V. Dolomanov, L. J. Bourhis, R. J. Gildea, J. A. K. Howard and H. Puschmann, *J. Appl. Crystallogr.*, 2009, **42**, 339–341.
7 C. Adamo and V. Barone, *J. Chem. Phys.*, 1999, **110**, 6158–6170.
8 S. Grimme, J. Antony, S. Ehrlich and H. Krieg, *J. Chem. Phys.*, 2010, **132**, 154104.
9 J. P. Merrick, D. Moran and L. Radom, *J. Phys. Chem. A*, 2007, **111**, 11683–11700.
10 Y. Chen, E. Trzop, A. Makal, J. D. Sokolow and P. Coppens, *Inorg. Chem.*, 2013, **52**, 4750–4752.
11 H.-T. Lv, Y. Cui, G.-D. Zou, N. Li, P. Yang and Y. Fan, *Dalton Trans.*, 2019, **48**, 14044–14048.
12 N. D. McNamara and J. C. Hicks, *ACS Appl. Mater. Interfaces*, 2015, **7**, 5338–5346.
13 Y. Zhang, G. Li, L. Kong and H. Lu, *Fuel*, 2018, **219**, 103–110.
14 S. Smolders, T. Willhammar, A. Krajnc, K. Sentosun, M. T. Wharmby, K. A. Lomachenko, S. Bals, G. Mali, M. B. J. Roeffaers, D. E. De Vos and B. Bueken, *Angew. Chem. Int. Ed.*, 2019, **58**, 9160–9165.
15 S. Yu, Y. Xiao, Z. Liu, J.-M. Lyu, Y.-L. Wang, Z.-Y. Hu, Y. Li, M.-H. Sun, L.-H. Chen and B.-L. Su, *Chem. Commun.*, 2023, **59**, 1801–1804.
16 G. Ye, Y. Sun, D. Zhang, W. Zhou, C. Lancelot, A. Rives, C. Lamonier and W. Xu, *Microporous Mesoporous Mater.*, 2018, **270**, 241–247.
17 G. Ye, Y. Gu, W. Zhou, W. Xu and Y. Sun, *ACS Catal.*, 2020, **10**, 2384–2394.
18 S. Lu, H. Zhong, D. Mo, Z. Hu, H. Zhou and Y. Yao, *Green Chem.*, 2017, **19**, 1371–1377.
19 G. Ye, H. Qi, X. Li, K. Leng, Y. Sun and W. Xu, *ChemPhysChem*, 2017, **18**, 1903–1908.
20 X. Li, Y. Mao, K. Leng, G. Ye, Y. Sun and W. Xu, *Microporous Mesoporous Mater.*, 2017, **254**, 114–120.
21 S.-T. Yang, K.-E. Jeong, S.-Y. Jeong and W.-S. Ahn, *Mater. Res. Bull.*, 2012, **47**, 4398–4402.
22 A. Chica, A. Corma and M. Domine, *J. Catal.*, 2006, **242**, 299–308.
23 C. Shi, W. Wang, N. Liu, X. Xu, D. Wang, M. Zhang, P. Sun and T. Chen, *Chem. Commun.*, 2015, **51**, 11500–11503.
24 K. Leng, X. Li, G. Ye, Y. Du, Y. Sun and W. Xu, *Catal. Sci. Technol.*, 2016, **6**, 7615–7622.
25 R. Bai, Q. Sun, Y. Song, N. Wang, T. Zhang, F. Wang, Y. Zou, Z. Feng, S. Miao and J. Yu, *J. Mater. Chem. A*, 2018, **6**, 8757–8762.
26 S. Yu, Z. Liu, J.-M. Lyu, C.-M. Guo, X.-Y. Yang, P. Jiang, Y.-L. Wang, Z.-Y. Hu, M.-H. Sun, Y. Li, L.-H. Chen and B.-L. Su, *Natl. Sci. Rev.*, 2024, **11**, nwae085.

27 X. Zhang, J. Zhang, J. Yin, X. Liu, W. Qiu, J. He, W. Jiang, L. Zhu, H. Li and H. Li, *Sep. Purif. Technol.*, 2025, **353**, 128289.
28 W. Song, D. Wang, X. Yue, C. Jin, Y. Wu, Y. Shi, J. Liu, A. Wu, C. Tian and H. Fu, *Inorg. Chem. Front.*, DOI:10.1039/D4QI02670E.
29 X. An, X. Gao, J. Yin, L. Xu, B. Zhang, J. He, H. Li, H. Li and W. Jiang, *Chem. Eng. J.*, 2024, **480**, 147879.
30 J. Zou, S. Wu, Y. Lin, X. Li, Q. Niu, S. He and C. Yang, *Environ. Sci. Technol.*, 2024, **58**, 14895–14905.
31 S. Gooneh-Farahani and M. Anbia, *J. Ind. Eng. Chem.*, 2025, **141**, 477–488.
32 Y.-L. Peng, J. Liu, H.-F. Zhang, D. Luo and D. Li, *Inorg. Chem. Front.*, 2018, **5**, 1563–1569.
33 Y. Xiao, N. Jiang, M. Liao, X. Pi, Z. Zhang, C. Peng, L. Zhang, H. Wu and J. Guo, *ACS Appl. Mater. Interfaces*, 2024, **16**, 63470–63481.
34 D. Shen, Y. Dai, J. Han, L. Gan, J. Liu and M. Long, *Chem. Eng. J.*, 2018, **332**, 563–571.
35 B. N. Bhadra, M. M. H. Mondol and S. H. Jhung, *Sep. Purif. Technol.*, 2024, **330**, 125425.
36 M. A. Hossain and S. H. Jhung, *Fuel*, 2024, **372**, 132178.
37 C. M. Granadeiro, S. O. Ribeiro, M. Karmaoui, R. Valença, J. C. Ribeiro, B. de Castro, L. Cunha-Silva and S. S. Balula, *Chem. Commun.*, 2015, **51**, 13818–13821.